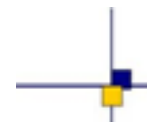


Validation of altimeter data by comparison with tide gauges measurements: yearly report 2016

for TOPEX/Poseidon, Jason-1, Jason-2, ERS-2, Envisat and SARAL/AltiKa

Contract No 14026/00 – 160182



Reference : CLS-DOS-17-0016

Nomenclature : SALP-RP-MA-EA-23082-CLS

Issue : 1 rev 1

Date : March 17, 2017



Chronology Issues:		
Issue:	Date:	Reason for change:
1.0	Jan, 5 th , 2017	Creation
1.1	Jan, 30 th , 2017	Delivery version
1.2	Mar, 18 th , 2017	Revised version

People involved in this issue:		
Written by:	P. Prandi V. Debout	CLS CLS
Checked by:	S. d'Alessio	CLS
Approved by:	J.P. Dumont M. Ablain	CLS
Application authorized by:		

Index Sheet:	
Context:	
Keywords:	
Hyperlink:	

Distribution:		
Company	Means of distribution	Names
CLS/DOS	1 electronic copy	M.ABLAIN
DOC/CLS	1 electronic copy	DOCUMENTATION
CNES	1 electronic copy	thierry.guinle@cnes.fr
CNES	1 electronic copy	aqgp_rs@cnes.fr
CNES	1 electronic copy	dominique.chermain@cnes.fr
CNES	1 electronic copy	delphine.vergnoux@cnes.fr

List of tables and figures

List of Tables

1	Multiple pixels improvements for the different altimetry missions compared to GLOSS/CLIVAR tide gauge network	29
2	Multiple pixels impact on the global drift between altimetry missions and the GLOSS/CLIVAR tide gauge network	30

List of Figures

1	<i>The triforme of Cal/Val activities for satellite altimetry missions</i>	1
2	<i>Acquisition procedure of tide gauges data into CLS database system.</i>	4
3	<i>Behaviour of the different low frequency filterings on missing points case. 10 % of the GC0001 hourly time serie is randomly removed by 10 measurements packs, the green crosses and circles are respectively the kept and removed data measurements. All the filtering methods are based on Demerliac coefficients and Dref is the reference, the filtered serie obtained from the full serie. Dold sets for the method used up to this year, Dnew sets for the basic method used now and Dcorr for the corrected filtering when tidal harmonic analysis is available.</i>	6
4	<i>Geographical distribution of GLOSS/CLIVAR tide gauges stations</i>	7
5	<i>Geographical distribution of PSMSL tide gauges stations</i>	8
6	<i>Geographical distribution of REFMAR tide gauges stations</i>	9
7	<i>Geographical distribution of CMEMS tide gauges stations</i>	10
8	<i>Geographical distribution of Senetosa tide gauges</i>	11
9	<i>General workflow of the altimetry versus tide gauges comparison process</i>	12
10	<i>Schematic representation of the pre-processing of satellite altimetry data</i>	13
11	<i>Schematic representation of the pre-processing of in-situ data</i>	14
12	<i>Schematic representation of the process used to generate colocated satellite altimetry and in-situ time series</i>	14
13	<i>Representation of the global averaging methodology</i>	16
14	<i>Monitoring of the number of tide gauges considered in the comparison between in-situ data and DUACS DT altimeter products</i>	17
15	<i>Time series of global average differences between Jason-2 and tide gauges, with (15a) and without the seasonal cycle (15b). The red points represent the raw data while the blue curve is obtained after applying a two months running mean filter</i>	18
16	<i>time series of global average differences between Jason-1 and tide gauges, with (16a) and without the seasonal cycle (16b). The red points represent the raw data while the blue curve is obtained after applying a two months running mean filter.</i>	19
17	<i>Time series of global average differences between TOPEX/Poseidon and tide gauges, with (17a) and without the seasonal cycle (17b). The red points represent the raw data while the blue curve is obtained after applying a two months running mean filter</i>	19
18	<i>Global mean differences for TOPEX/Poseidon, Jason-1 and Jason-2, each mission limited to the period over which it is used as the GMSL reference</i>	20
19	<i>Time series of global average differences between SARAL/Altika and tide gauges, with (19a) and without the seasonal cycle (19b). The red points represent the raw data while the blue curve is obtained after applying a two months running mean filter</i>	21

.....

20	<i>Time series of global average differences between ENVISAT and tide gauges, with (20a) and without the seasonal cycle (20b). The red points represent the raw data while the blue curve is obtained after applying a two months running mean filter . . .</i>	21
21	<i>Time series of global average differences between ERS-2 and tide gauges, with (21a) and without the seasonal cycle (21b). The red points represent the raw data while the blue curve is obtained after applying a two months running mean filter</i>	22
22	<i>Time series of global average differences between SSALTO/DUACS maps of SLA and tide gauges keeping (left) or removing (right) the seasonal cycle. The red points represent the raw data while the blue curve is obtained after applying a two months running mean filter</i>	23
23	<i>Drift of the Alti-TG serie (GLOSS/CLIVAR) as a function of the bin shape used. From left to right and top to bottom: TOPEX-Poseidon, Jason-1, Jason-2, CMEMS DT.</i>	25
24	<i>Stability of the Alti-TG drift serie (GLOSS/CLIVAR) as function of the bin shape used. It is statistically determined using a Monte Carlo scheme to evaluate the standard deviation of the distribution of any subset of the stations set. For each subset, 10 % of the stations are randomly taken out. From left to right and top to bottom: TOPEX-Poseidon, Jason-1, Jason-2, CMEMS DT.</i>	26
25	<i>Correlation between tide gauge and altimetry series as a function of the number of pixels averaged for altimetry. The different curves set for the 10 first stations of the GLOSS/CLIVER network compared to Jason-1 altimetry grids.</i>	27
26	<i>Utilization of multiple pixels for the comparison between Jason-1 altimetry grids and GLOSS/CLIVAR network. On the left, the tide gauge distribution of the number of pixels averaged to get the maximal correlation (N_{max}). On the right, the tide gauge distribution of the correlation increase from single pixel ($N = 1$) to multiple pixel ($N = N_{max}$).</i>	28
27	<i>Comparison of PSMSL and GLOSS/CLIVAR drifts derived from altimetry - tide gauges. Each subplot sets for an altimetry mission. On the left, the reference missions TOPEX/Poseidon, Jason-1, Jason-2 from top to bottom. On the right, the long cycle mission ERS-2, Envisat, SARAL/Altika from top to bottom.</i>	31
28	<i>Number of valid tide gauges versus the distance limit of colocation for GLOSS/CLIVAR (left) and PSMSL (right).</i>	32
29	<i>Mean correlation of valid tide gauges versus the distance limit of colocation for GLOSS/CLIVAR (left) and PSMSL (right).</i>	33
30	<i>Variation of the GMSL drift between altimetry and tide gauges for GLOSS/CLIVAR (left) and PSMSL (right). On top, the trend obtained by linear regression and on bottom, the trend formal uncertainty.</i>	33
31	<i>Ground motion infered from DInSAR in Manila over the 1993-1998 period from [31].</i>	35
32	<i>Comparing global bias times series for the current TOPEX/Poseidon record, and for a Poseidon calibrated TOPEX record.</i>	36
33	<i>Altimetry Standards</i>	42

List of items to be defined or to be confirmed

Applicable documents / reference documents

Contents

1	Introduction	1
2	Database: a review of tide gauges datasets in use	3
2.1.	Overview	3
2.2.	Acquisition	3
2.3.	Post-processing	4
2.3.1.	High frequency signals removal	5
2.3.2.	Vertical motion of the tide gauge benchmark	5
2.4.	Tidal networks	6
2.4.1.	GLOSS/CLIVAR network	6
2.4.2.	PSMSL database	8
2.4.3.	REFMAR database	9
2.4.4.	CMEMS dataset	10
2.4.5.	Senetosa tide gauges	11
3	Methodology: a careful description of the altimeter/tide gauges comparison procedure	12
3.1.	Overview	12
3.2.	Pre-processing of altimetry and in-situ data	13
3.2.1.	Satellite altimetry data	13
3.2.2.	Tide gauge data	14
3.3.	Station-wise comparison between altimetry and tide gauge data	14
3.3.1.	Temporal resampling	15
3.3.2.	Correlation estimation, quality check and extraction	15
3.3.3.	Referencing of tide gauges time series	15
3.4.	Computation of global statistics	15
4	Detection of drifts and jumps on global altimeter records	17
4.1.	Jason-2	18
4.2.	Jason-1	18
4.3.	TOPEX/Poseidon	19
4.4.	TOPEX/Jason historical ground track	20
4.5.	SARAL/Altika	20
4.6.	ENVISAT	21
4.7.	ERS-2	21
4.8.	SSALTO/DUACS maps of Sea Level Anomaly	22
5	Particular investigations	24
5.1.	Ensemble Mean Estimation	24
5.2.	Multiple pixel utilization	27
5.3.	Comparison between PSMSL and GLOSS/CLIVAR	30
5.4.	Distance threshold	32
5.5.	SAR interferometry for VLM characterisation	35
5.6.	Drift of a Poseidon based TOPEX record	36
6	Conclusions	37
7	References	39

.....

8 Appendix	42
8.1. Standard DUACS 2014	42

1. Introduction

This document is the altimeter/tide gauges comparison activities synthesis report for the year 2016. It sums up the activities performed in the frame of the 2016-2019 SALP project funded by CNES.

Methods used for the calibration and validation of satellite altimetry data can be separated in three broad categories, which are graphically summarized as the *CalVal triforme* (see figure 1). These three categories are:

- mono-mission analysis where the internal consistency of one mission is assessed,
- multi-mission analysis which cross-compares two or more altimeter missions to check for any drifts or biases,
- comparisons with in-situ data which provide an external, independent reference.

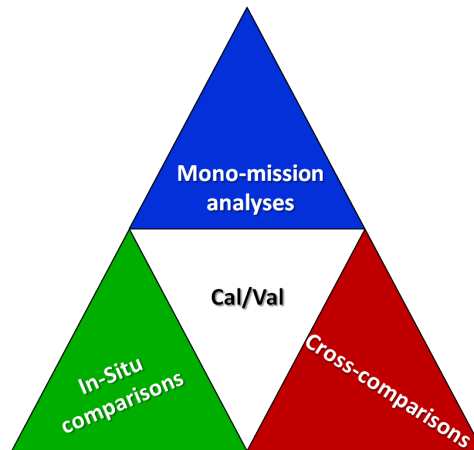


Figure 1: The triforme of Cal/Val activities for satellite altimetry missions

In the present report we focus on the third category of Cal/Val activities, and more specifically on comparisons between satellite altimetry and tide gauges. Comparisons between satellite altimeter data and tide gauges are performed by several teams, and the methods used can be divided into two categories:

- comparisons at dedicated calibration sites where one (or a few) carefully monitored in-situ sensor is used, with the aim of detecting offsets and long-term drifts of altimeter missions. Such sites are rare (Harvest, Senetosa and Bass Strait) and generally dedicated to the validation of one mission (orbit dependent),
- global comparisons using a wide network of tide gauges (generally more than 100 sites) distributed over the entire ocean. From this ensemble of local altimetry/in-situ comparisons, global averages are estimated.

At CLS, we use a global altimetry/tide gauges comparison method which falls in the second category of these techniques: a global difference is estimated at each time step from a network of in-situ stations. This way of processing data is replicated for all altimetry cycles to build global average time series. These time series, along with other statistics, are used for three main goals:

1. Detect drifts, shifts and any regime changes in the altimeter sea level time series
2. Estimate improvements provided by new altimeter standards (orbit solution, geophysical corrections...) on the SSH consistency between altimetry and tide gauges
3. Perform a quality control of the in-situ time series, where drifts and jumps can remain with no physical signification (drift of sensors, anthropogenic sources ...)

For the last three years, tide gauges activities at CLS have been driven by the recommendations of the OST/ST community in 2013 that the different groups involved in such comparisons should document their methods and provide reliable estimates of uncertainties, as well as work together to explain the observed discrepancies between results. In 2016, the work performed on this activity has followed two different axes,

- an in-depth revamp of the database management and acquisition tools, as well as some in-situ processing upgrades, which are described in sections 2 and 3,
- a sequel to the sensitivity studies of the last two years adressing the impact of different processing choices in section 5.

Of course comparisons between satellite altimetry missions and tide gauges stations are performed routinely and updated time series of biases are provided in section 4.

2. Database: a review of tide gauges datasets in use

2.1. Overview

The tidal database aggregates tide gauges Sea Surface Height (SSH) records from different stations. The stations are generally distributed through networks which aim to provide a uniform dataset (with respect to file format, conventions, ...). Several geophysical corrections such as pressure and wind effects are applied on the raw data, and tidal effects are filtered in order to deduce Sea Level Anomalies (SLA) from tide gauges consistent with altimeter data. Building the tide gauges database is therefore the first step, and an essential one, of the altimetry versus tide gauges comparison process.

This year the acquisition and the processing of tide gauges data has been globally revised in order to work uniformly on all the networks, and to provide a more consistent output across networks. This effort to increase robustness follows the identification of a weak spot in our previous data acquisition methods, which could lead to corruption of our internal database when applied to unstable network repositories (*ie* repositories with stations going in and out for example). Now, the in-situ database is operationnally updated with data from five tide gauges networks which are described below (2.4.). This database is separated in three sub-bases, according to data sampling rate:

- a *monthly* database for PSMSL network,
- a *high rate* database containing all original series whose sampling period is shorter than one hour.
- an *hourly* database aggregating all stations of all networks, resampled if the original sampling is not hourly,

The general workflow of tide gauges acquisition and processing is schematically displayed on figure 2, and the different processing steps are described in the sub sections below. Concerning the re-sampling, the high-rate data is binned in time along an hourly sampling. All the measurements in the hourly bin are averaged with equal weights. By filtering the hourly time serie, a correction is obtained to remove high frequency. This correction is propagated on the high rate time serie (original sampling) using a linear interpolation between the measurements of the hourly time serie. On the other hand, an hourly sampling is also computed from the monthly time series of PSMSL network. The hourly time serie is linearly interpolated between the monthly measurements which are corrected in order to conserve the original monthly means. Note that these hourly series are artificial and should not be used for comparison with altimetry, but they may be compared to the time series of duplicated stations in other networks in order to investigate on the signal information lost by the PSMSL monthly averaging.

The tide gauges database is updated every week.

2.2. Acquisition

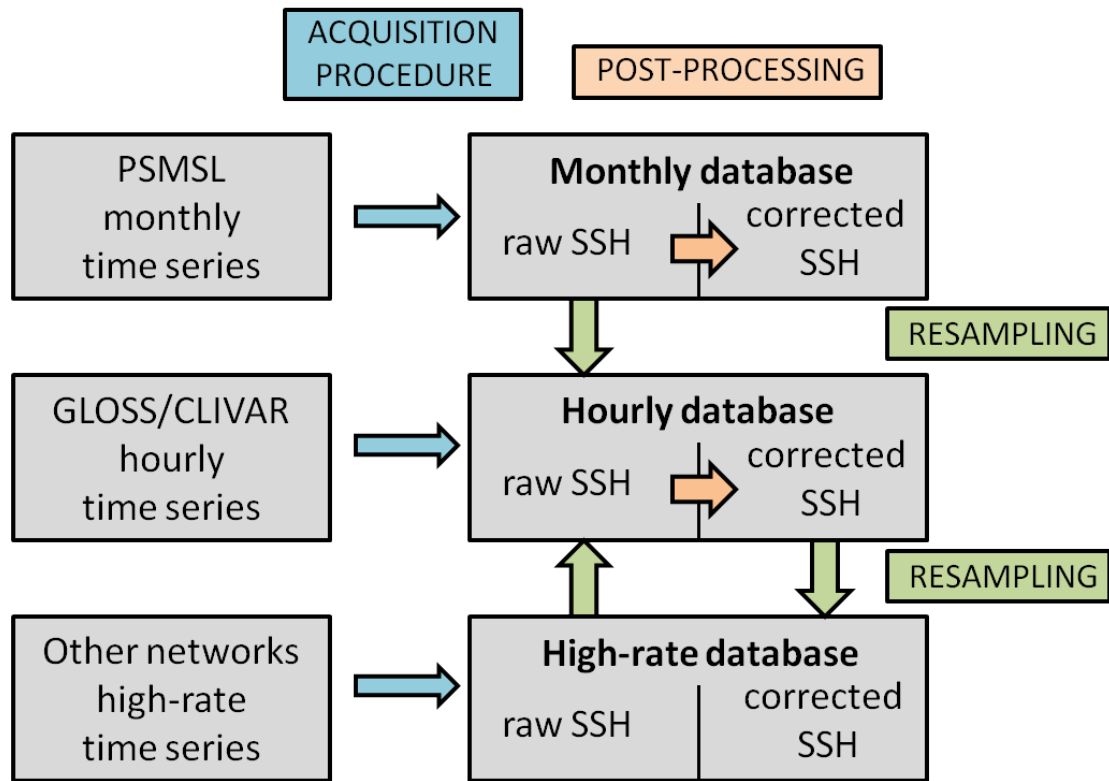


Figure 2: Acquisition procedure of tide gauges data into CLS database system.

For the different tidal networks used at CLS (see section 2.4.), we routinely check the data provider servers for data updates. New data are downloaded and converted into CLS internal format to update our database. At this step, the raw sea surface height and some static information are acquired (network, sensor code, sensor coordinates, quality flags, ...). In 2016, we had to face several events regarding data retrieval from external servers leading to acquisition errors on CLS side, and a delay on the update of our databases. Despite efforts to make the acquisition programs more robust to events on the data providers' side, these remain the main source of issues and delays.

A quality flag is now associated to each individual in-situ SSH measurement. It is constructed from the quality checks provided by the different networks to indicate if the measurement can be used or not in the post-processing. If no quality information is available, then measurements are considered valid.

2.3. Post-processing

After downloading and converting in-situ SSH measurements into our database, several post-processing steps are applied to the data to enrich the raw in-situ SSH values and make them comparable with satellite altimetry data:

1. filtering of tide gauge data to remove tidal signals, this induces a resampling for non hourly measurements,
2. interpolation of the high resolution dynamical atmospheric correction (MOG2D model) at the time and position of the measurement,

3. interpolation of a model for local GIA-induced vertical land motion.

2.3.1. High frequency signals removal

High frequency tidal effects on tide gauges data are corrected using the Demerliac low-pass filter [5, Bessero, 1985]. Long period tidal waves are also corrected using a specific algorithm based on well-balanced tide tables [10, Cartwright and Eden, 1973]. High frequency atmospheric effects are corrected by withdrawing the Mog2d Dynamical Atmospheric Correction (DAC) (Dorandeu and Le Traon, 1999 [12]; Carrere and Lyard, 2003 [9]). Note that the correction applied also contains the inverse barometer effect.

This year we improved the low-pass Demerliac filter algorithm in order to reduce the impact of missing points. Demerliac filter coefficients are based on an hourly sampling period. Up to now, missing points in time series were lineary interpolated. The new filtering method uses the results of an harmonic analysis of the in-situ SSH signal to extrapolate missing values, and falls back to not using missing points at all when no harmonic analysis results are available. The latter happens for short, incomplete or displaying large errors (steps, drifts) time series. Such time series represent less than 5 % of the tide gauges database.

Figure 3 compares the results of the old and new methods on a time series where missing points were artificially created. The old method (labeled Dold) results in differences that can reach up to ≈ 0.2 m when missing points are concentrated at the minimum or the maximum of the tidal variations, and the global RMS of the differences with the reference is 3.1 cm. When no harmonic analysis results are available, the new method (labeled Dnew) reduce local differences to 0.1 m and the RMS of the differences drops to 1.9 cm. However when harmonic analysis results are available, the method (labeled Dcorr) is able to reduce local differences down to 0.01 m while the RMS of the differences is only 0.02 m.

Moreover we apply a hourly downsampling to measurements of high rate stations, and therefore apply the Demerliac filter to the downsampled time series. The results are backward propagated to high rate data again, which allows to remove tidal signals from high rate data. This is a significant improvement, as it makes fully corrected high rate data available, as well as increases the number of stations in the hourly database.

2.3.2. Vertical motion of the tide gauge benchmark

One large uncertainty concerning tide gauge data is the vertical stability of the tide gauge benchmark over time. Vertical motions of tide gauges benchmarks can be monitored accurately using geodetic techniques such as DORIS or GPS levelling. In fact, only a few stations are associated with such monitoring devices. As a consequence, we are not able to correct all tide gauges for vertical motions of the benchmark derived from GPS or DORIS data.

One part of crustal motions is the response of the Earth's crust to the last deglaciation (known as GIA), which can induce large vertical motions. Models are available to estimate this effect, and predict vertical land motion rates over the globe. We use the ICE-5G/VM4 model [15, Peltier, 2004] to correct tide gauges time series for vertical land motion due to GIA. The last version of

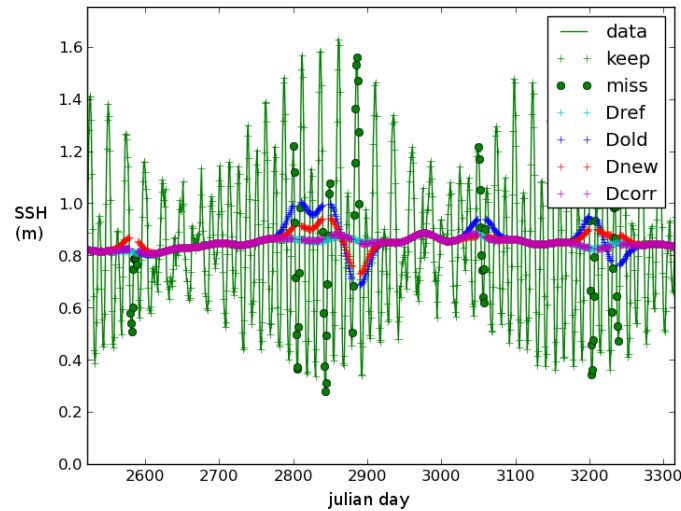


Figure 3: Behaviour of the different low frequency filterings on missing points case. 10 % of the GC0001 hourly time serie is randomly removed by 10 measurements packs, the green crosses and circles are respectively the kept and removed data measurements. All the filtering methods are based on Demerliac coefficients and **Dref** is the reference, the filtered serie obtained from the full serie. **Dold** sets for the method used up to this year, **Dnew** sets for the basic method used now and **Dcorr** for the corrected filtering when tidal harmonic analysis is available.

this model named ICE-6G(VM5a) [16, Peltier, 2015] is available and has to be tested.

Regarding this issue, section 5.5. suggests that even GPS and/or DORIS stations may not be able to measure actual tide gauge datum movement in many cases, due to local geological features, and that SAR interferometry provides a useful tool for ground motion retrieval.

2.4. Tidal networks

This section presents the tidal networks currently available in the tide gauges database at CLS. The historical tidal database consisted in different tide gauges networks resulting from different collaborations. The data covered different time periods and were used for various kind of scientific studies. With the same goal, the current database is now routinely updated with two global tidal networks (GLOSS/CLIVAR and PSMSL). Three additional networks are also acquired, but their coverages are not as complete than the two previous ones.

2.4.1. GLOSS/CLIVAR network

The GLOSS/CLIVAR (Global Sea Level Observing System/Climate Variability and Predictability) network is currently the most useful network for Cal/Val activities. It provides time series of 290 tide gauge stations, with an hourly temporal sampling. These measurements are used for tide prediction as well as altimetry validation. We use the fast delivery dataset to benefit from the

short delay between sensing time and delivery time. Data are retrieved through the University of Hawaii Sea Level Center (UHSLC) ftp server at <ftp.soest.hawaii.edu/uhs/c/woce/>. The current geographical distribution of the GLOSS/CLIVAR data is displayed on figure 4.

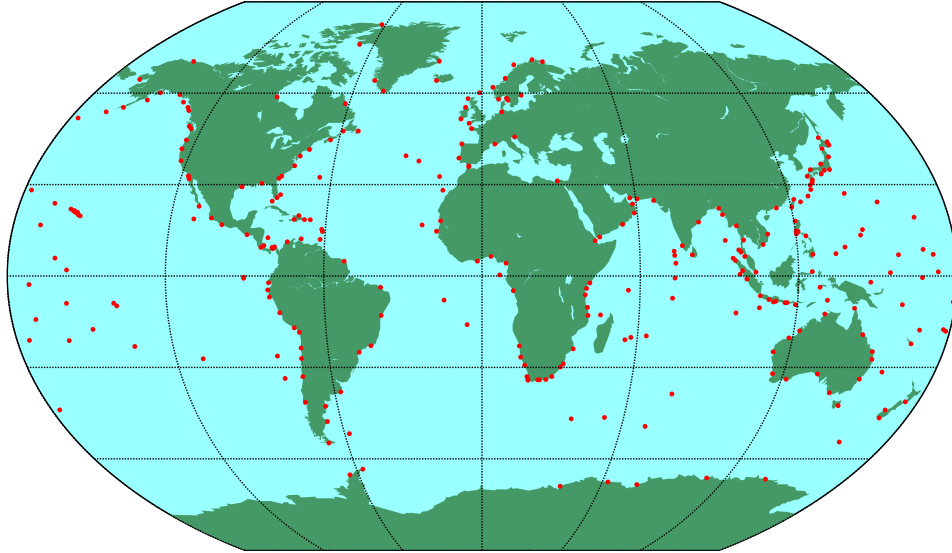


Figure 4: Geographical distribution of GLOSS/CLIVAR tide gauges stations

2.4.2. PSMSL database

The Permanent Service for Mean Sea Level (PSMSL) maintains a large historical database which contains more than 1350 tide gauges. Monthly averages of SSH are provided, with no higher frequency available. Data are retrieved monthly through the PSMSL website at <http://www.psmsl.org>, but the delivery delay is generally much longer than for the GLOSS network. The geographical coverage of this network is displayed on figure 5. It should be noted that the global spatial distribution along the coastline is not as homogeneous as GLOSS/CLIVAR one. Moreover a lot of stations time series are not suitable for global comparisons to altimeter (ends before TOPEX/Poseidon mission, contains lot of steps in serie, duplicate another station...).

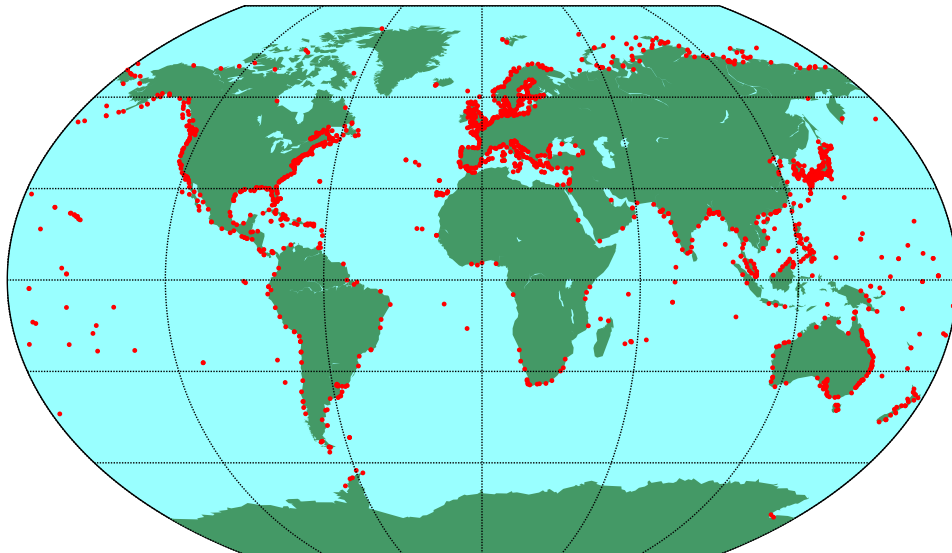


Figure 5: Geographical distribution of PSMSL tide gauges stations

2.4.3. REFMAR database

The acquisition of the REFMAR database is conducted since 2014. This is a French database operated by SHOM (<http://refmar.shom.fr>). The REFMAR time series have a 10 minutes sampling. They are downloaded weekly from the SHOM servers. The geographical coverage of this network is mainly restricted to french coasts and displayed on figure 6.

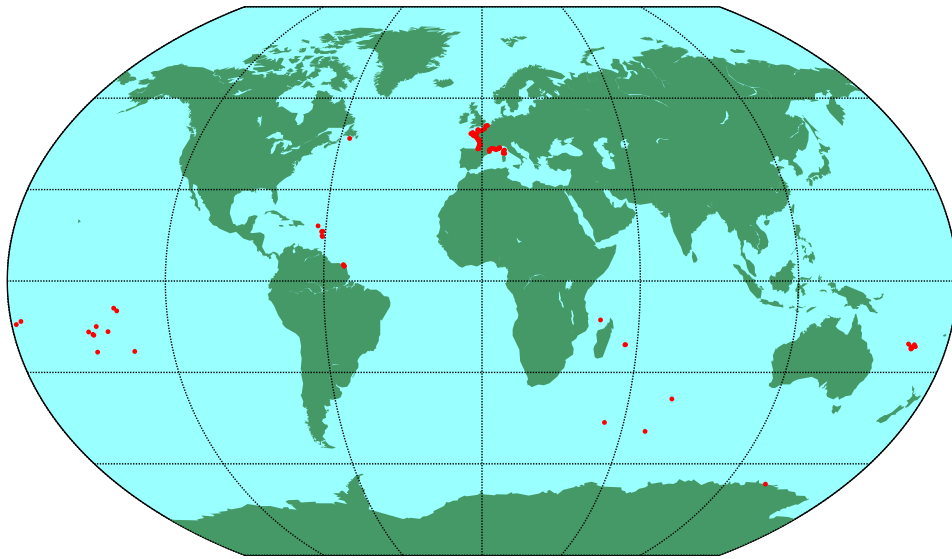


Figure 6: Geographical distribution of REFMAR tide gauges stations

2.4.4. CMEMS dataset

Tide gauges time series are delivered daily by IFREMER in the framework of the CMEMS (Copernicus Marine Environment Monitoring Service) project. For data validation purposes, we perform daily acquisitions of this data but do not use these data for Cal/Val activities yet. The distribution of the CMEMS network is displayed on figure 7.

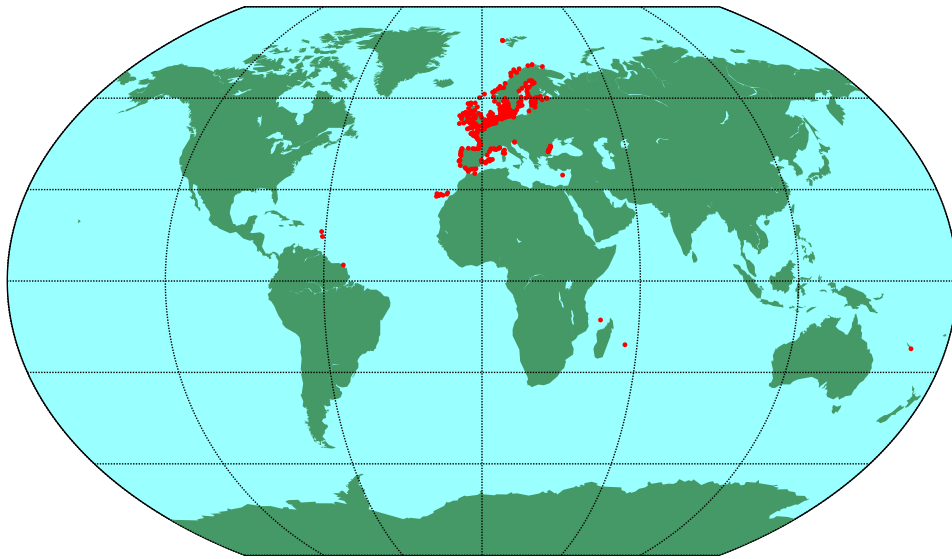


Figure 7: Geographical distribution of CMEMS tide gauges stations

2.4.5. Senetosa tide gauges

Note that the Senetosa tide gauge time series of the M3, M4, M5 and M7 sensors are made available through the AVISO website (www.aviso.oceanobs.com), where the in-situ section is divided into 2 parts, one concerning the absolute calibration and the other dedicated to the global comparison with altimetry. All these sensors are located in Corsica, as shown on the map for figure 8.

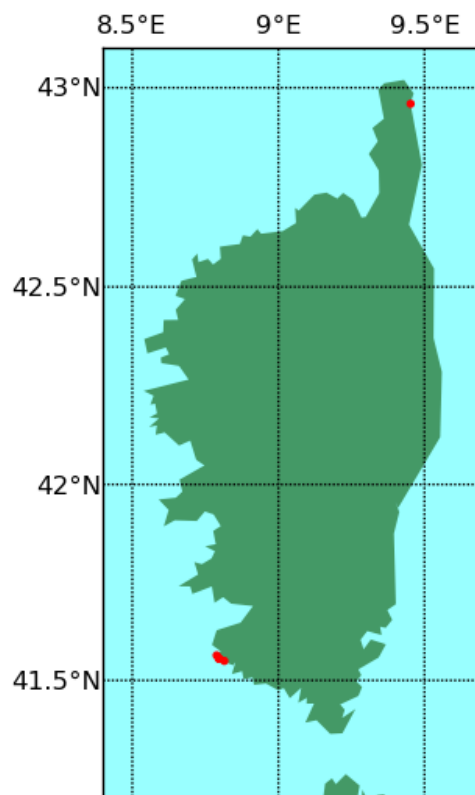


Figure 8: Geographical distribution of Senetosa tide gauges

3. Methodology: a careful description of the altimeter/tide gauges comparison procedure

3.1. Overview

In the present section of this report, we provide a careful description of the processing used at CLS to compare altimetry data to in-situ measurements from tide gauges.

As the SLA is now properly computed on all the networks, the major change of this year is the ability to compare any station of any network to altimetry one. Nevertheless, GLOSS/CLIVAR is still the most reliable and relevant network for the Cal/Val needs and only the results of the comparison between this network and the tide gauges are detailed in this section. Beside this, the processing is very similar as the last year one and only little changes have been made to this section.

Different schematic representations of the processing are used to ease the description. We used a consistent representation rule to display the different elements of the processing:

- processing steps that imply a transformation of the input data are displayed as rectangles,
- processing steps that do not transform the input data are displayed as diamonds,
- the original databases are displayed as tube sections (rectangles with curved vertical sides),
- intermediate datasets are displayed as parallelograms.

Figure 9 displays a schematic overview of the processing:

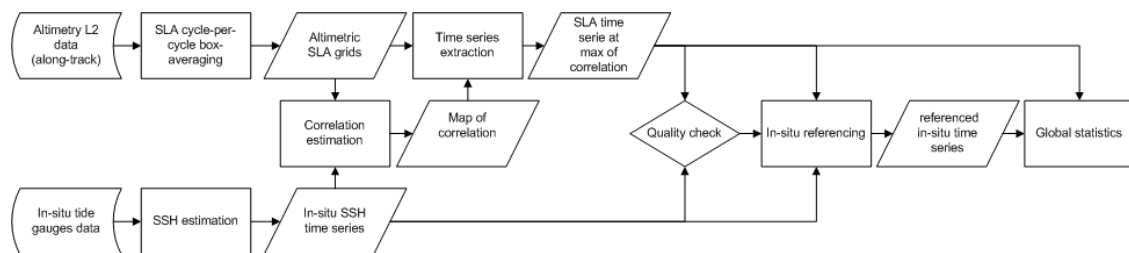


Figure 9: General workflow of the altimetry versus tide gauges comparison process

The major steps of this processing are:

- the pre-processing of altimetry and tide gauge data to derive sea level anomalies,
- the computation of correlation maps between altimetry and tide gauges,
- the extraction of a satellite altimetry time serie for each tide gauge station,
- the referencing of the tide gauges time series with respect to altimetry data,
- the estimation of global statistics.

The five steps of the processing listed above are described with more details in the sections of the present chapter.

3.2. Pre-processing of altimetry and in-situ data

3.2.1. Satellite altimetry data

Radar altimeters provide Sea Surface Heights (SSH), which need to be referenced and corrected from geophysical signals to provide Sea Level Anomalies (SLA) comparable with in-situ measurements. Concerning altimeter data, along-track (level 2) SSH from several satellite altimeters are considered, for which standards are updated following the Geophysical Data Record (GDR) altimeter products. The Sea Level Anomalies (SLA) are computed from the along-track data according to equation 1:

$$SSH = Orbit - Altimeter\ Range - \sum_{i=1}^n Correction_i - Mean\ Sea\ Surface \quad (1)$$

where the corrections applied are:

$$\begin{aligned} \sum_{i=1}^n Correction_i = & \text{Dry troposphere correction} \\ & + \text{Dynamic atmospheric correction} \\ & + \text{Wet troposphere correction} \\ & + \text{Ionospheric correction} \\ & + \text{Sea state bias correction} \\ & + \text{Ocean tide} \\ & + \text{Solid earth tide} \\ & + \text{Geocentric pole tide} \end{aligned}$$

For more details about the actual corrections used in the SLA calculation for each altimeter (for example the model used for ocean tide estimation), please refer to [21]. In practice, the geophysical corrections used are consistent with the one used to estimate the global Mean Sea Level (MSL). Only valid measurements are considered, relying on a Cal/Val flag to perform this selection. Along-track SLA are then averaged on a regular 1° by 1° grid, with a temporal sampling corresponding to each mission's repetitivity.

The pre-processing applied to level 2 satellite altimetry data is summarized on figure 10.

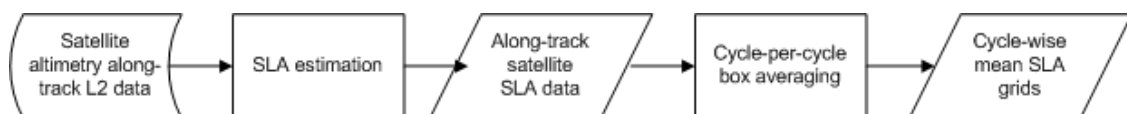


Figure 10: Schematic representation of the pre-processing of satellite altimetry data

3.2.2. Tide gauge data

The goal of this pre-processing is to extract a corrected sea surface height time series, at each tide gauge station, with a physical content comparable to the satellite altimetry one. Nevertheless, the relative sea surface heights measured by tide gauges are different from absolute sea surface heights obtained by satellite altimeters. Therefore the pre-processing applied to in-situ measurements differs from the satellite altimetry one.

The first difference is that tide gauges were designed to estimate tides and, as a consequence, generally have a much higher sampling rate than satellite altimetry records. Typically, tide gauges would sample the ocean every hour while, at a given point, the satellite altimetry sampling is higher than ten days. The second difference results from the fact that tide gauges measure the sea surface height relative to an on-ground benchmark. Every movement of this local datum has a direct effect on sea level measurements.

The pre-processing applied to in-situ measurements from tide gauges is summarized on figure 11. The method for removing high frequency signals is described in section 2.3.1. while the correction of vertical land motion is described in section 2.3.2..

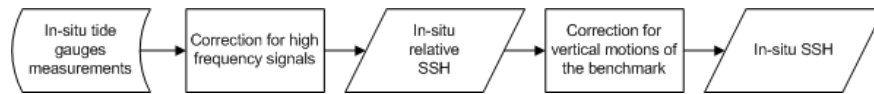


Figure 11: Schematic representation of the pre-processing of in-situ data

3.3. Station-wise comparison between altimetry and tide gauge data

At this point of the processing workflow, both altimeter and tide gauges data show comparable SSH physical contents. The next step of the comparison process is to extract one satellite altimetry time series at each tide gauge site. The process used to extract the altimetry time series and to generate colocated time series at each tide gauge station is schematically described on figure 12. This processing is applied for each tide gauge station in the database, and the different steps involved are described in the present section.

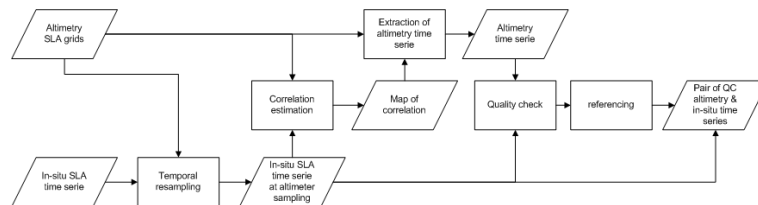


Figure 12: Schematic representation of the process used to generate colocated satellite altimetry and in-situ time series

3.3.1. Temporal resampling

The temporal sampling of satellite altimetry corresponds to the repetitivity of the mission, while tide gauge measurements generally have a much higher temporal. Before performing any comparison between the two measurements, high frequency tide gauge data are resampled at the low frequency of the altimetry data by performing averages over one altimeter cycle window.

3.3.2. Correlation estimation, quality check and extraction

After resampling the tide gauge time series, a map of the correlation coefficients between altimetry grids and the in-situ record is computed. Note that the tide gauge time series has to contain at least 2 years of measurements for the correlations to be estimated.

The satellite altimetry time series is then extracted where the maximum of correlation is found within a 200 km distance from the tide gauge. The distance of 150 km used last year has been increased as it appeared too small in some cases with respect to the altimeter spatial sampling. Along the equator, the spatial sampling of altimetry grids is indeed about 110 km and inter-track distance is about 160 km for Topex/Poseidon and Jason satellites. A 200 km radius ensures that any tide gauge can be effectively compared to the two closest tracks. A specific investigation has been performed to evaluate the impact of this parameter on global statistics (see section 5.4.).

Only satellite time series defined on more than 80 % of the tide gauge time series are eligible. If no altimetry serie fulfills this condition, the station is not considered in the global comparison.

3.3.3. Referencing of tide gauges time series

An important step of the processing is to reference tide gauge time series onto altimetry ones. Tide gauge measurements are referenced with respect to a local benchmark, whose position is generally given within the frame of a national datum system. In this processing, satellite altimetry is considered as a model for in-situ data to be referenced into a common frame. Therefore, the mean of the altimetry-TG SSH differences is computed and subtracted from each tide gauge time series.

3.4. Computation of global statistics

The main goal of the comparison procedure is to generate global statistics between altimetry and in-situ measurements, able to indicate any global drift of the level-2 satellite altimeter data.

At this moment, a set of pairs of colocated altimetry and in-situ time series has been produced. A further selection is operated to keep only the pairs fulfilling the following criteria:

- the correlation between altimetry and tide gauge time series is higher than 0.7,
- the standard deviation of the differences between altimetry and tide gauge data does not exceed 10 cm,

The aim of this last step of the processing is to generate one global time series of the differences between altimetry and in-situ from the larger set of colocated time series. This is performed by

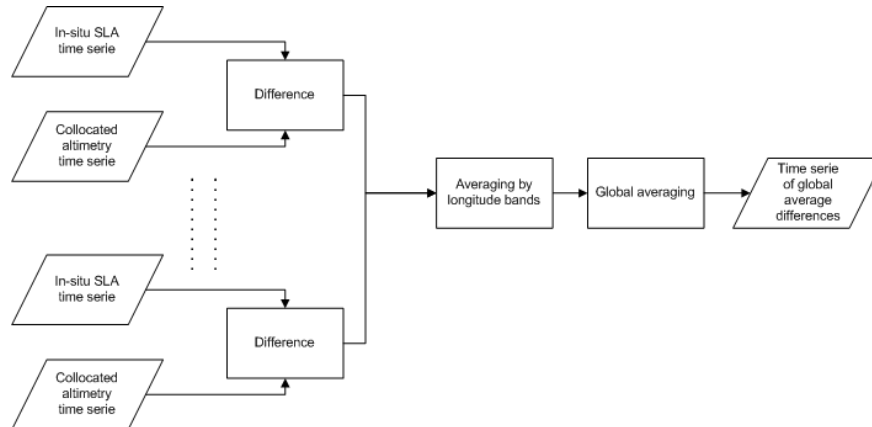


Figure 13: Representation of the global averaging methodology

averaging all records together.

Tide gauges stations are unevenly distributed along the global coastline, and some regions (like the European Atlantic coasts) are oversampled while other areas (such as the Southern Ocean) are almost not observed. In order to mitigate the effects of this uneven sampling, the global mean average is estimated through a two step process:

- data are averaged first on 6° wide longitude bands,
- longitude bands are then averaged into the global mean.

The averaging method used to compute global mean time serie from a set of colocated altimetry and tide gauges time series is schematically displayed on figure 13.

4. Detection of drifts and jumps on global altimeter records

The cycle by cycle monitoring of global average differences between altimetry and in-situ sea surface height measurements provides a way to assess the satellite data quality and to detect jumps and drifts affecting sea level records.

In this section, tide gauges from the GLOSS/CLIVAR database are compared to level-2 altimeter records. However due to the quality criteria that are applied, the average number of stations retained in each point of comparison may vary significantly. Indeed, the number of tide gauges considered differs from one altimetry mission to another, and, over time for a given mission, depending on the availability of the in-situ sensors. The evolution of the number of tide gauges used in the global average estimation is represented on figure 14. While an almost linear growth of the number of tide gauges, corresponding to the availability of new stations in the dataset, is displayed for the most part of the time period, a slight decrease can be observed at the end due to the time lag of the update of tide gauge measurements in the database. The corrections used to compute the altimetry SLA of the different missions are detailed annex 8.1..

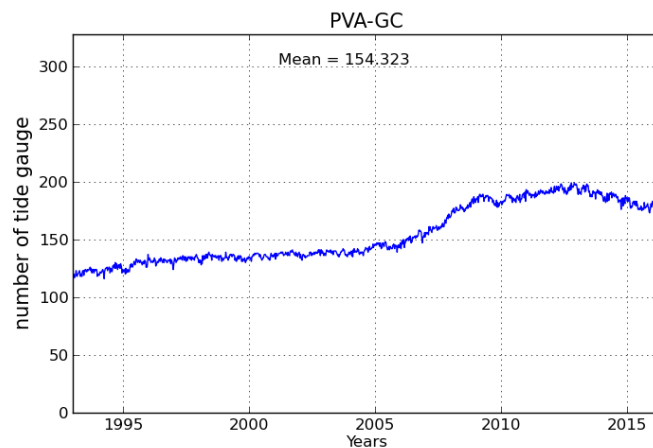


Figure 14: Monitoring of the number of tide gauges considered in the comparison between in-situ data and DUACS DT altimeter products

Note that all the global mean differences time series presented in this section have been corrected for GIA effects on satellite altimetry data using a uniform -0.3 mm/year trend correction. The details of this GIA correction can be found in the 2013 annual report for the altimetry/tide gauges global comparisons [20].

4.1. Jason-2

Figure 15 displays the time series of global average differences between Jason-2 and tide gauges, either keeping (15a) or removing the seasonal cycle (15b).

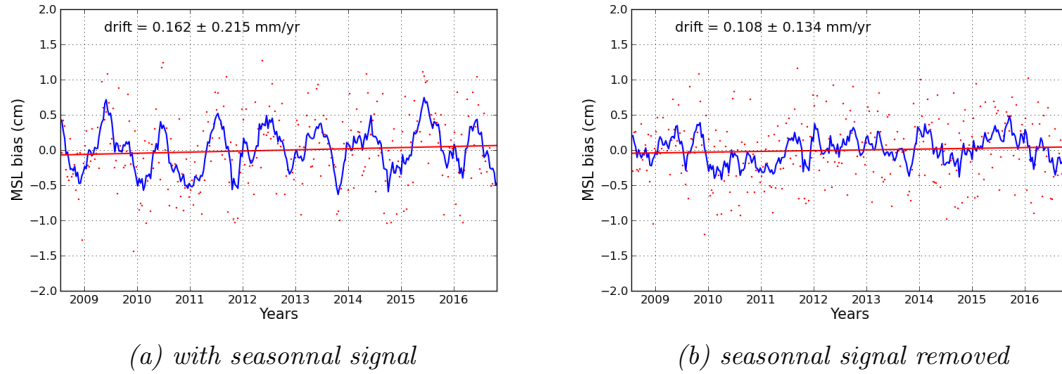


Figure 15: Time series of global average differences between Jason-2 and tide gauges, with (15a) and without the seasonal cycle (15b). The red points represent the raw data while the blue curve is obtained after applying a two months running mean filter

Considering both curves, Jason-2 shows a remarkable agreement with tide gauges measurements (drift lower than ≈ 0.1 mm/year). The formal linear regression uncertainty is small, 0.13 mm/year, but due to all the process steps, the actual error of the method may be larger, up to 0.7 mm/year according to [24, (Valladeau et al., 2012)]. As a recent mission, Jason-2 benefits of numerous tide gauges stations to be compared to (≈ 200 fulfilling the criteria). Overall, figure 15 confirms the excellent stability of the Jason-2 mission with respect to tide gauges.

4.2. Jason-1

Figure 16 displays the time series of global average differences between Jason-1 and tide gauges, either keeping (16a) or removing the seasonal cycle (16b). Considering both curves, although the comparison with tide gauges reveals a 0.3 mm/year drift greater than the regression uncertainty, it remains relatively weak and is not sufficient to conclude on a real long-term trend differences.

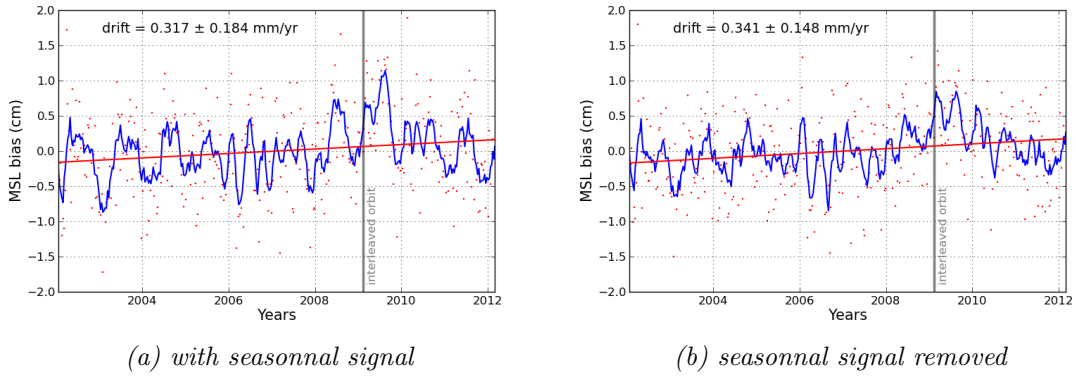


Figure 16: time series of global average differences between Jason-1 and tide gauges, with (16a) and without the seasonal cycle (16b). The red points represent the raw data while the blue curve is obtained after applying a two months running mean filter.

Due to the changing point of closest approach and therefore altimetry/in-situ collocation during Jason-1 geodetic phase, this phase (from May 2012 onward) has been removed from the analysis. A small bias is still noticeable at the change between the nominal and interleaved orbits. This bias might result from two effects: either there is a true bias between the two phases of the mission or the different ground tracks imply that the series of the altimetry grid cells are not consistent enough on the full period.

4.3. TOPEX/Poseidon

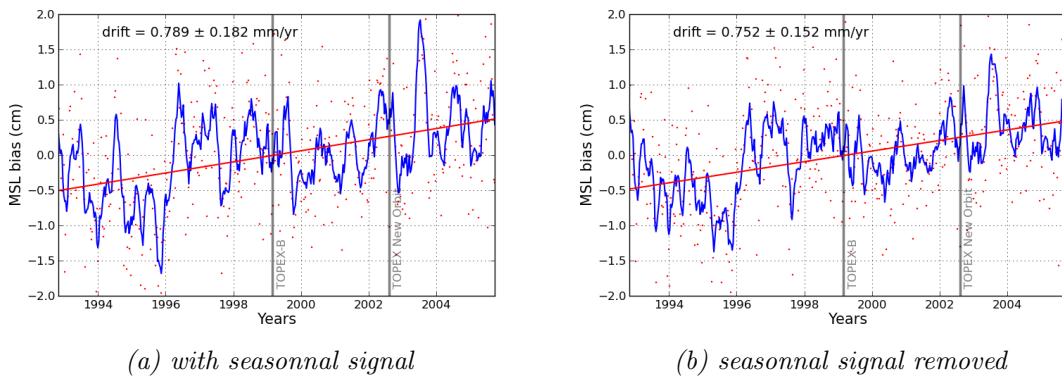


Figure 17: Time series of global average differences between TOPEX/Poseidon and tide gauges, with (17a) and without the seasonal cycle (17b). The red points represent the raw data while the blue curve is obtained after applying a two months running mean filter

Since T/P space mission delivered one of the longest available altimeter time series, the comparison with tide gauges has become of reference regarding studies about MSL drift. Results on the differences between T/P data and tide gauges measurements (figure 17) display a global positive trend of about 0.7 mm/yr over the 1993-2005 time period. Furthermore, the low drift uncertainty (< 0.2 mm/yr) is in favor of a reliable assessment of T/P global MSL on the whole altimeter time period. However, focusing on both TOPEX-A (cycles 11 to 236) and TOPEX-B (cycles 237 to 364) time periods, the behavior of the altimeter is quite different. The significant positive drift detected

on TOPEX-A from 1996 onwards corresponds to the beginning of the TOPEX-A anomaly (cycles 130 to 236) when strong instrumental instabilities have been highlighted on significant wave height, range and backscatter coefficient parameters (Ablain et al., 2012 [1]). The TOPEX-B MSL appears more stable with no drift from February 1999 onwards. Although T/P seems to provide accurate measurements for climate studies, the long-term stability of TOPEX-A data could be improved.

At the OST/ST meeting in La Rochelle, [32, Beckley et al., 2016] investigated the effect of the cal-mode on the TOPEX/Poseidon GMSL record. The impact of this correction is consistent with the signal observed in 1995-1996 in global comparisons with tide gauges.

4.4. TOPEX/Jason historical ground track

In the sections above, we considered separately, and over their longest period the three missions used to construct the GMSL record. But one important concern when comparing altimetry to tide gauges is to assess whether the 20+ years long GMSL record from TOPEX/Poseidon, Jason-1 and Jason-2 is stable over time. Figure 18 displays the global mean alti minus tide gauges differences for these three missions limited to the individual period they are used as reference mission for the GMSL record.

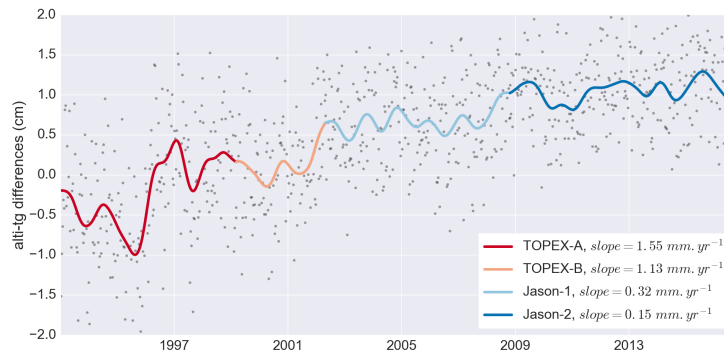


Figure 18: Global mean differences for TOPEX/Poseidon, Jason-1 and Jason-2, each mission limited to the period over which it is used as the GMSL reference

The positive drift observed on TOPEX/Poseidon global differences with in-situ (1.2 mm/yr) suggests that on the TOPEX/Poseidon period, the altimetry record might be overestimating the GMSL rise. This is consistent with findings by other groups ([28]). Concerning Jason-1 and Jason-2 compared to tide gauges, the respectively 0.21 mm/yr and -0.34 mm/yr drifts are smaller.

Overall the global curve seems to have a concave behaviour suggesting that drift difference between altimetry reference mission and tide gauge is reversing. Nevertheless, one has to remember that the tide gauge dataset enriched a lot from TOPEX/Poseidon to Jason-2, doubling the number of stations fulfilling criteria from ≈ 100 to ≈ 200 stations. This trend may then be due to a spatial sampling bias.

4.5. SARAL/Altika

Figure 19 displays the results of the global bias estimation with respect to tide gauges for the SARAL/AltiKa mission. The 3 years of altimetry data are not sufficient to have an accurate linear regression. Thus the 0.6 mm/year drift uncertainty is still large despite a very reduced RMS of differences between altimetry and tide gauges. The estimated drift is around 0.3 mm/year which is not significant. These results suggest a good stability of SARAL/AltiKa with respect to tide gauges.

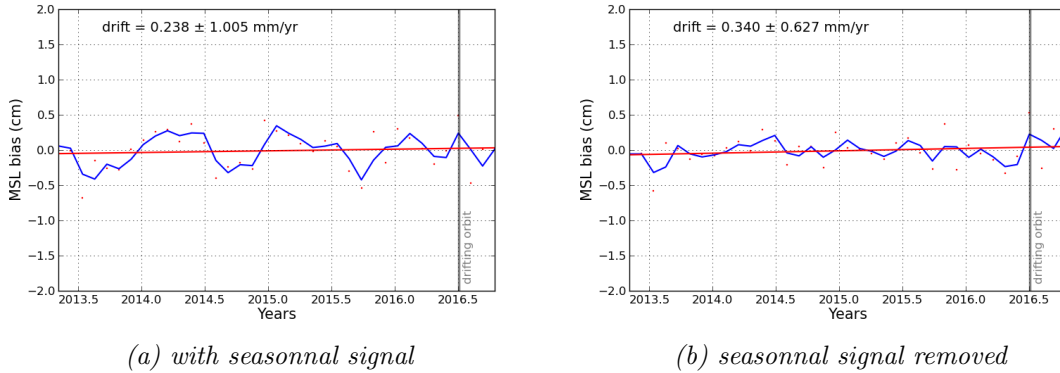


Figure 19: Time series of global average differences between SARAL/AltiKa and tide gauges, with (19a) and without the seasonal cycle (19b). The red points represent the raw data while the blue curve is obtained after applying a two months running mean filter

4.6. ENVISAT

Figure 20 displays the results of the global bias estimation between the altimetre ENVISAT mission and tide gauges. Compared to reference missions, ENVISAT has a larger SSH differences drift at 0.9 mm/yr. This value is above the method uncertainty and therefore statistically significant. Moreover, such a drift is consistent with comparisons between Jason-1 and ENVISAT on the global MSL.

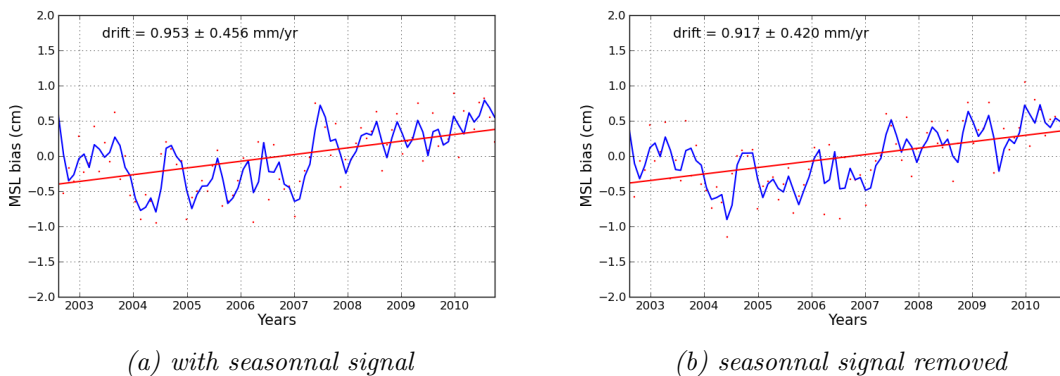


Figure 20: Time series of global average differences between ENVISAT and tide gauges, with (20a) and without the seasonal cycle (20b). The red points represent the raw data while the blue curve is obtained after applying a two months running mean filter

4.7. ERS-2

Figure 21 displays the results of the global bias estimation with respect to tide gauges for the ERS-2 mission. Compared to reference missions, ERS-2 shows larger negative SSH differences drift at ≈ -1 mm/yr. This is consistent with comparisons between TOPEX/Poseidon and ERS-2 on the global MSL. The linear regression hardly fits what seems to be long term oscillation of the trends.

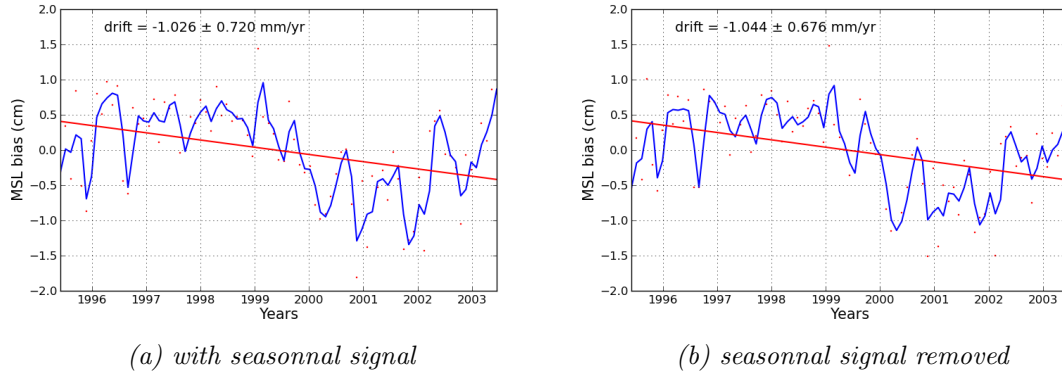


Figure 21: Time series of global average differences between ERS-2 and tide gauges, with (21a) and without the seasonal cycle (21b). The red points represent the raw data while the blue curve is obtained after applying a two months running mean filter

4.8. SSALTO/DUACS maps of Sea Level Anomaly

Analysing multi-mission datasets provides a way to study long, homogeneous time series. In this section we present the activities performed over the last year regarding the comparison of the so-called "value added" products to in-situ SSH measurements from tide gauges. Figure 22 displays the time series of the global biases between DUACS multi-mission product and tide gauges. The variability of the bias is higher at the beginning of the period, and consistent with the comparison between TOPEX and tide gauges, as TOPEX/Poseidon is the reference mission at the beginning of the record.

A global 0.37 mm/year drift difference is found between DUACS multi-mission product and tide gauges trends. This matches with the average drift obtained for the different reference missions (see figure 18). While it appears significant with respect to the 0.03 mm/year uncertainty of the linear regression, please note that the total uncertainty of the method is greater than this due several error sources that are not accounted for in a formal linear regression error.

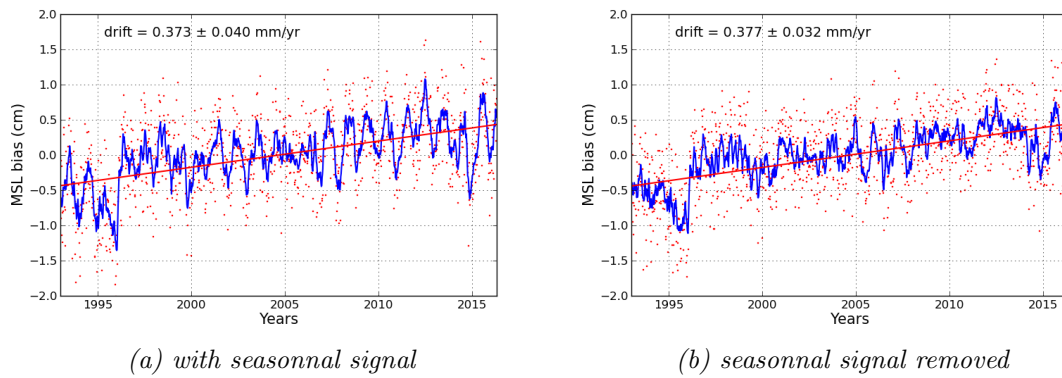


Figure 22: Time series of global average differences between SSALTO/DUACS maps of SLA and tide gauges keeping (left) or removing (right) the seasonal cycle. The red points represent the raw data while the blue curve is obtained after applying a two months running mean filter

5. Particular investigations

In October 2013, the OSTST community recommended that the different groups should intercompare their methodologies with two goals:

- understand the origin of the differences observed on the global results,
- come to a better knowledge of the sensitivity and uncertainty of the method.

This type of sensitivity testing had begun on CLS side in 2013 when we addressed GIA corrections and was continued in 2014 focusing on two axes:

- the impact of correcting or not for the annual signal in altimetry and in-situ time series when estimating the correlations,
- the effects of including incomplete time series in our analysis rather than rejecting all stations that do not cover the whole period of the study.

The results can be found in the previous yearly reports for the activity [20] and [21].

In 2015 the averaging process and its uncertainty was investigated, results are detailed in last year's report [22] and suggested that both the set of stations and the averaging method may have a significant impact on the drift estimation. In 2016 we build up on investigations performed over the last two years, and make an effort to estimate more precisely the sensitivity of the method. These investigations are detailed below and include:

- an impact assessment of the boxes size of the averaging,
- a new colocation method based on multiple pixels in order to reduce the signal to noise ratio of time series,
- a comparison between drifts obtained with GLOSS/CLIVAR and with PSMSL tide gauges networks,
- an assessment of the impact of extending the colocation radius.

5.1. Ensemble Mean Estimation

As discussed in last years' report [22], the way to average individual time series of differences into one global record may impact largely the resulting global drift. The current method at CLS is to average all stations in 6° longitudinal bands and then average the longitudinal bands together. The goal is to reduce the effect of residual signals, such as GIA related ones, on a non homogeneous station distribution. Different authors propose a different averaging scheme:

- Watson [28] uses an uncertainty-based weighting scheme (more consistent tide gauges are favored),
- Jevrejeva [29] uses regional averages through an iterative virtual station method.

Here we investigate how the global drift varies with the averaging bin size. The "bin size" corresponds to the latitude/longitude step used to mesh the Mercator projection. The difference series

are averaged in each cell of the grid before the cells are averaged together. Therefore the current method is equivalent to $180^\circ/6^\circ$ bins.

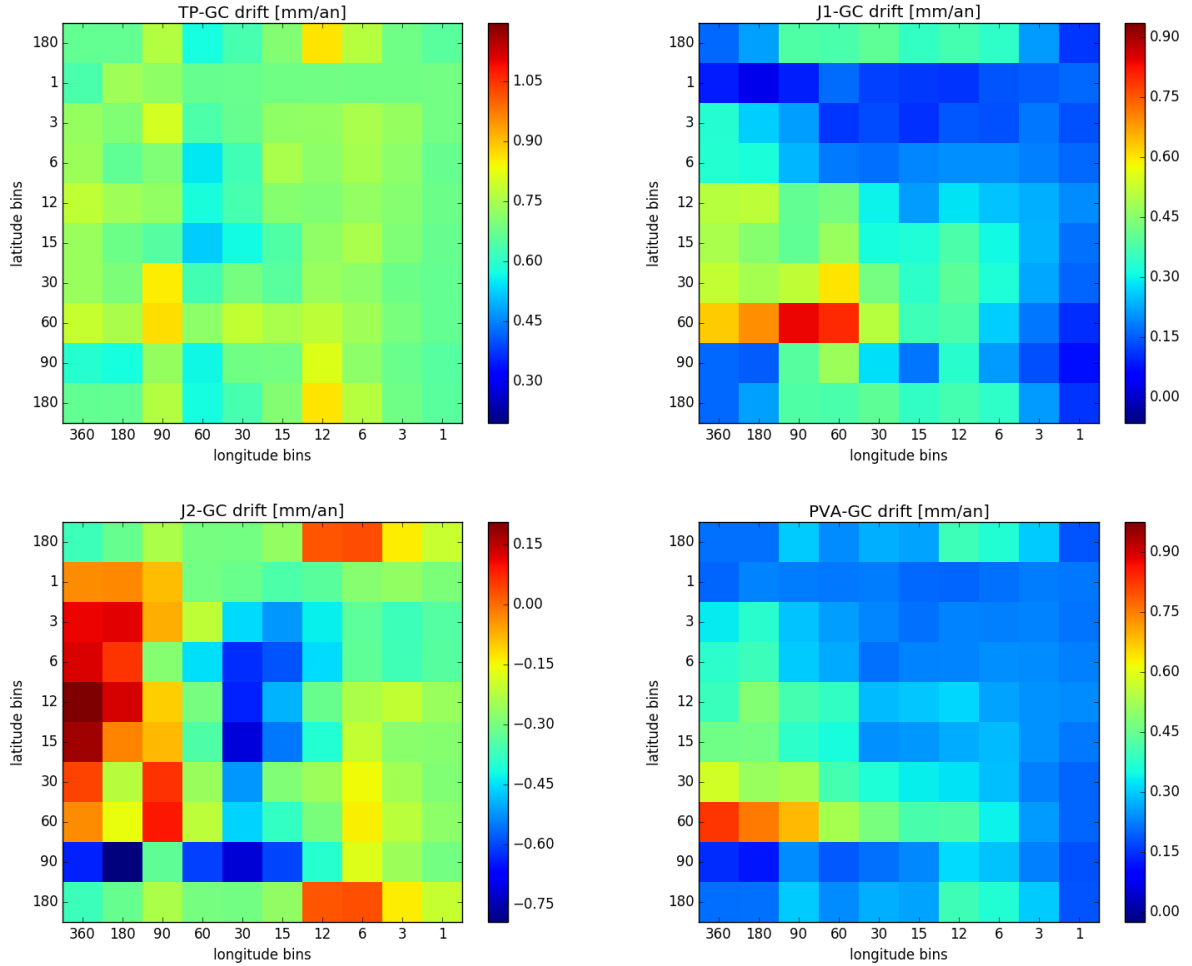


Figure 23: Drift of the Alti-TG serie (GLOSS/CLIVAR) as a function of the bin shape used. From left to right and top to bottom: TOPEX-Poseidon, Jason-1, Jason-2, CMEMS DT.

Figure 23 shows the drifts obtained on the Alti-TG averaged serie for the different bin shapes. One should notice that the drift varies on a 0.28 mm/year range for TOPEX/Poseidon, which is relatively stable, whereas for Jason-1, Jason-2 and CMEMS DT, the variation ranges are 0.8, 0.9 and 0.64 mm/year respectively. The bin shape chosen does have a strong impact on the resulting drift.

The true drift is of course unknown and there is no direct metric to determine which of those bin shape is the most accurate. However, the role of the longitude bands is to resorb the effect of the non homogeneous station distribution along the coastline, and a “good” bin shape should be insensitive to small changes in the network. Figure 24 displays the uncertainties associated to the drifts of figure 23. These are estimated through a Monte Carlo experiment randomly removing a fraction (10%) of the stations from the analysis. On all missions, larger uncertainties are found in the same zone, corresponding to large bin sizes (around 90° by 60° boxes). Observed uncertainties depend

.....

on the length of the time series but always remain below 0.5 mm/year, for more stable bins they are around 0.25 mm/year for mono-mission analysis. The best results in terms of drift uncertainty are obtained, at least for mono-mission analysis, for small bins of about $6^\circ \times 6^\circ$ latitude \times longitude. The 6° longitude case currently used for global comparisons is rather stable, < 0.3 mm/year for mono-mission and < 0.06 mm/year for CMEMS DT.

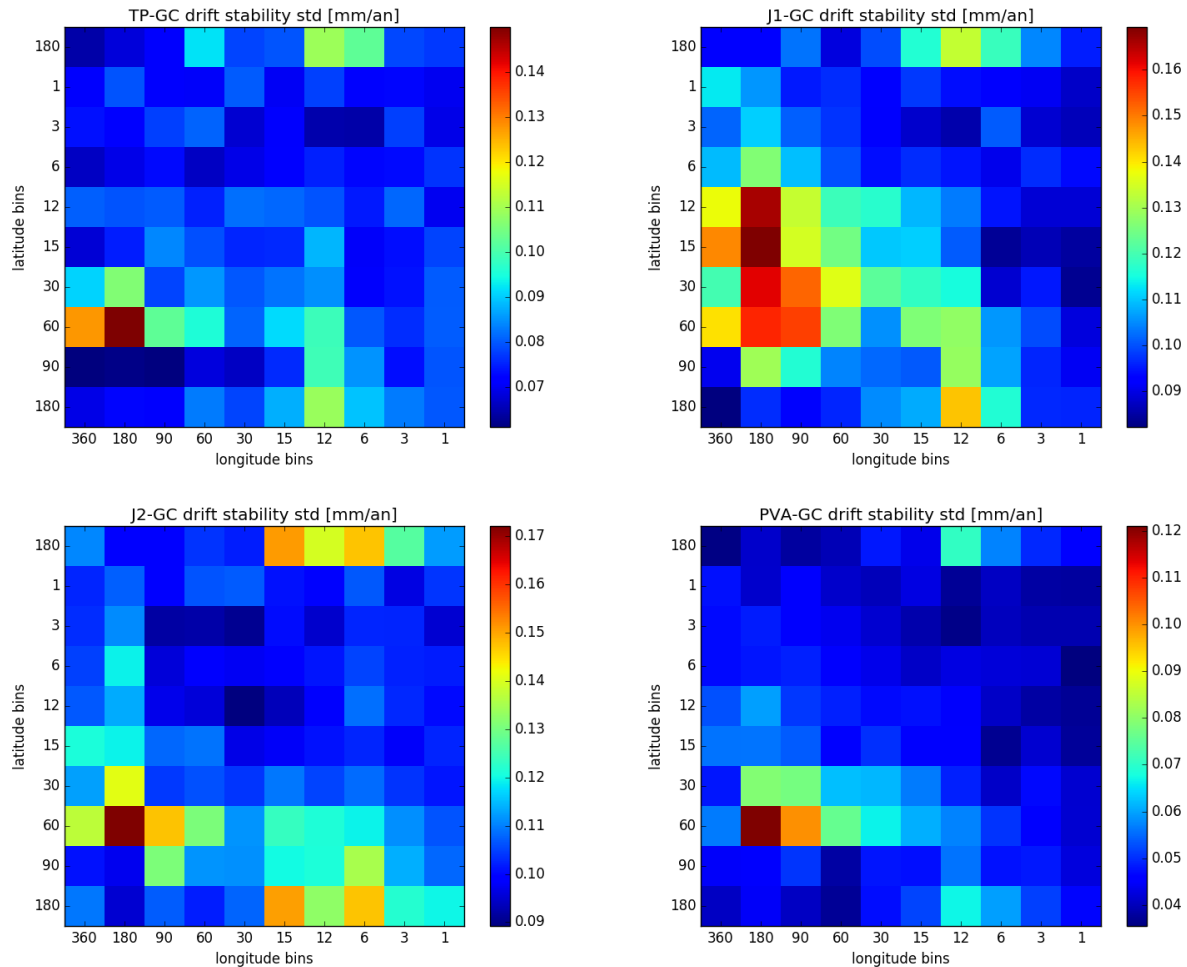


Figure 24: Stability of the Alti-TG drift serie (GLOSS/CLIVAR) as function of the bin shape used. It is statistically determined using a Monte Carlo scheme to evaluate the standard deviation of the distribution of any subset of the stations set. For each subset, 10 % of the stations are randomly taken out. From left to right and top to bottom: TOPEX-Poseidon, Jason-1, Jason-2, CMEMS DT.

As a conclusion, we demonstrate here that bin shape affects the drift between altimetry and tide gauges to a large extent. It is also clear that some bin shapes should be avoided for exemple big latitude bands which are very unstable. The current 6° longitude bands appears to be a good compromise even if more stable bin shapes exist like small latitude and longitude bins.

5.2. Multiple pixel utilization

Colocated altimeter time series are extracted at the position of highest correlation. Therefore all the other altimeter series are not considered afterward, even if the map of correlations shows several pixels with similar correlation values. Here we investigate the possibility to use several altimeter data points to estimate colocated altimeter time series. Noise levels on both series are responsible for a part of the discrepancies between tide gauges and altimetry. By averaging the series of the first altimeter pixels in terms of correlation, altimeter noise level is expected to be reduced.

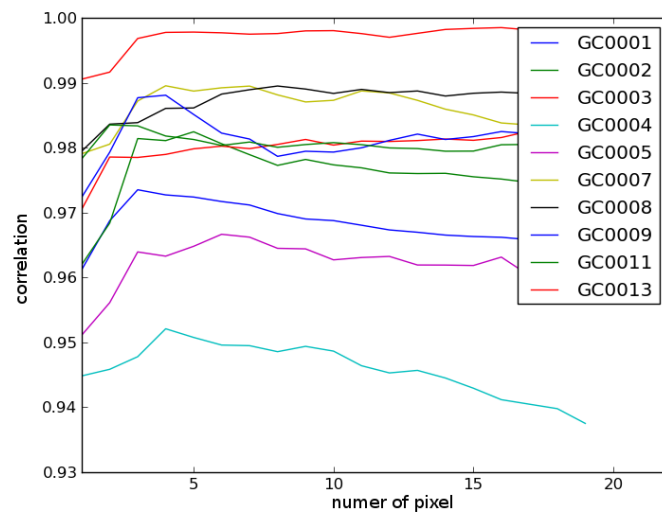


Figure 25: Correlation between tide gauge and altimetry series as a function of the number of pixels averaged for altimetry. The different curves set for the 10 first stations of the GLOSS/CLIVER network compared to Jason-1 altimetry grids.

Figure 25 shows how the correlation between the altimeter and tide gauges time series varies with the number of pixels averaged. The N pixels picked are the N first one in terms of individual correlation with tide gauge serie. All 10 stations presented here already have a very good correlation with one pixel (> 0.94). Nevertheless, it is clear that whatever the sensor, the correlation improves at first when N increases. This remains true up to a value of $N = N_{max}$ depending on the sensor (see below). This may be interpreted as averaging out of the altimetry noise level by increasing the amount of measurements.

Passed N_{max} , the correlation decreases as N increases with a variable slope depending on the station. This may be due to the lack of additional pixels with an altimetry signal consistent with the tide gauge serie. The SLA altimetry signal in the pixels used have a more and more significant physical difference with the tide gauge serie. Therefore, the improvement on the altimetry noise does not compensate this loss.

Figure 26 left shows the distribution of the N_{max} values of the GLOSS/CLIVAR tide gauges compared to Jason-1. On the 243 tide gauges, there are 60 which have no interest in using multiple pixels ($N_{max} = 1$). Most of tide gauges have a N_{max} value between 1 and 5 and only 3 tide gauges have $N_{max} > 10$. This may be variable with the grid refinement and the maximum distance fixed

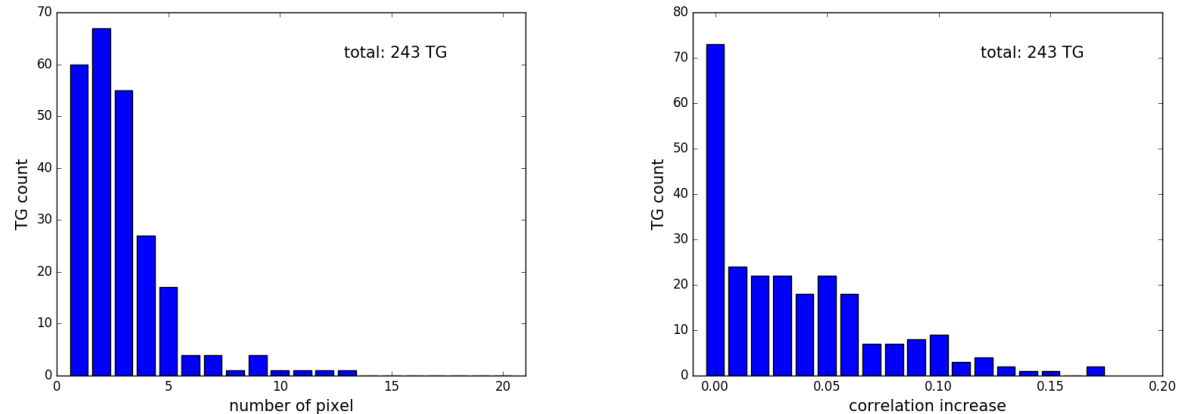


Figure 26: Utilization of multiple pixels for the comparison between Jason-1 altimetry grids and GLOSS/CLIVAR network. On the left, the tide gauge distribution of the number of pixels averaged to get the maximal correlation (N_{max}). On the right, the tide gauge distribution of the correlation increase from single pixel ($N = 1$) to multiple pixel ($N = N_{max}$).

between altimetry and tide gauge. Hereinafter, the test on N values is limited to $N \leq 10$.

Figure 26 right presents the distribution of the increase of correlation for the same altimetry-tide gauge set (Jason-1 - GLOSS/CLIVAR). One has to note that this increase sets for the use of N_{max} which, by its definition, can only have a better correlation than a single pixel. 73 tide gauges do not have a significantly better correlation ($\Delta C < 0.01$), among them are the 60 having $N_{max} = 1$. For most of the others, the correlation enhancement is between 0.01 and 0.06 but it may be up to 0.17.

The multiple pixel technique is applied, as a test, to global comparisons for the different altimetry missions with respect to the GLOSS/CLIVAR tide gauge network. The performance of this method is evaluated on different metrics:

- the number of tide gauges passing the validity thresholds (correlation > 0.7 and DRMS < 10 cm),
- the average correlation altimetry/tide gauge of all the stations available on the mission period,
- the average DRMS altimetry/tide gauge of all the stations available on the mission period,

The results are summarized in table 1. Note that the 'long cycle' missions based on a 35 days repetitivity cycle (ERS 2, Envisat, Saral/Altika) naturally have less noisy grids than the 'short cycle' missions with a 10 days repetitivity cycle (TOPEX/Poseidon, Jason-1, Jason-2). Moreover, as the formers use 1002 tracks cycle, they have denser grids than the latters using only 254 tracks per cycle. This explain the better mean correlations and mean DRMS obtained for the long cycle missions.

The multiple pixels method provides some improvements. It increases the number of valid tide gauges by 10-15 % for short cycle missions and by 3-5 % for long cycle missions. All missions benefit of a 0.35-0.45% increase of the mean correlation demonstrating the true ability of the multiple pixels method to reduce the signal to noise ratio of the altimetry-tide gauge comparison. Concerning the DRMS, the reduction is around 0.6 cm for the short cycle missions representing 10-12 % of the DRMS obtained with a single pixel. Whereas the long cycle missions have a 0.7 cm decrease

Altimetry mission	TG number			Correlation		DRMS (cm)	
	available	$N = 1$	$N = N_{max}$	$N = 1$	$N = N_{max}$	$N = 1$	$N = N_{max}$
TOPEX/Poseidon	182	97	116	0.654	0.689	6.62	5.98
Jason-1	243	153	174	0.712	0.749	5.99	5.28
Jason-2	264	198	213	0.774	0.809	5.53	4.91
ERS 2	185	148	156	0.773	0.819	4.69	3.85
Envisat	238	195	202	0.806	0.849	4.22	3.49
Saral	239	202	211	0.824	0.864	4.50	3.79

Table 1: Multiple pixels improvements for the different altimetry missions compared to GLOSS/CLIVAR tide gauge network. The improvements are between the single pixel use ($N = 1$) and the multiple pixels use ($N = N_{max}$) in terms of number of valid tide gauges (correlation > 0.7 DRMS < 10 cm), mean correlation and mean DRMS. The "available" sub column of "TG number" sets for the number of tide gauges that are comparable to this mission (time serie length > 2 years and at least one valid altimetry pixel in the 200 km radius). Note that the mean correlations and DRMS are computed on all these available tide gauges.

reaching 15-19 % of the initial DRMS.

The impact on the global drift between altimetry and GLOSS/CLIVAR tide gauges was also evaluated for every mission. Table 2 gathers the evolution of the trend and its uncertainty (formal here) when passing from the single pixel to the multiple pixels use. The drift of the multiple pixels method was computed for the same set of stations (no new stations added) and for an extended set containing the new stations passing the thresholds thanks to the new method.

One should note that the uncertainties on the drift is larger for the long cycle mission (0.5-1 mm/year instead of 0.1 mm/year). As their grids are 35 days averages, they indeed have much less measurement points to constrain the linear regression. Furthermore, their time series are generally shorter than the short cycle missions, especially for Saral/Altika having less than 4 years of data.

The multiple pixels method does not significantly modify the drift. The most impacted missions are Jason-1, Envisat and Saral/Altika drift difference of up to 0.3 mm/year with respect to single pixel. For Jason-1, it even represents more than the regression uncertainty. For the other missions, the drift change is smaller than 0.1 mm/year. The results do not allow to make a conclusion on which of the individual station DSLA evolution by averaging several pixels and the growth of the station set is responsible of this difference as it depends on the altimetry mission. Nevertheless, the slope uncertainty shows a global reduction for each of these two steps for the short cycle mission (the total effect is around 10 %). For the long cycle mission, the result is more variable with even a 10 % rise of the uncertainty for Saral/Altika.

Altimetry mission	drift (mm/year)			drift uncert. (mm/year)		
	N	N_{max}^{same}	N_{max}^{all}	1	N_{max}^{same}	N_{max}^{all}
TOPEX/Poseidon	0.752	0.799	0.657	0.152	0.143	0.140
Jason-1	0.341	0.152	0.167	0.148	0.132	0.129
Jason-2	0.108	0.102	-0.005	0.134	0.119	0.120
ERS 2	-1.044	-1.109	-1.072	0.676	0.696	0.603
Envisat	0.953	0.633	0.522	0.456	0.493	0.488
Saral	0.340	0.194	0.494	0.627	0.628	0.663

Table 2: Multiple pixels impact on the global drift between altimetry missions and the GLOSS/CLIVAR tide gauge network. The values are given for a single pixel use ($N = 1$), the multiple pixels ($N = N_{max}$) use on the same set of stations (the single pixel valid ones) and the multiple pixels use on the full set of valid stations. The drift is computed once the annual signal is removed and the uncertainty is the 3σ formal error estimated of the linear regression.

5.3. Comparison between PSMSL and GLOSS/CLIVAR

The PSMSL tide gauges network contains a huge pool of tide gauges even if we are not as confident on the data quality of every individual tide gauge as we are for GLOSS/CLIVAR. The PSMSL time series are distributed with a monthly time sampling. Therefore, another serie of monthly altimetry grid is created for each mission. It actually changes the sampling for TOPEX/Poseidon, Jason-1 and Jason-2. For ERS-2, Envisat and SARAL/Altika, the change is lighter but the grid follow calendar months rather than cycles.

The world distribution of PSMSL tide gauges (figure 5) is less homogeneous than GLOSS/CLIVAR one (figure 4) with far more stations in the northern hemisphere. Therefore, the altimetry-tide gauges drifts derived with PSMSL and GLOSS/CLIVAR are compared to investigate on a possible regional bias it would imply. The results are presented on figure 27. Note that PSMSL data are generally distributed with a longer time delay than GLOSS/CLIVAR. Furthermore, PSMSL is corrected with the ERA-interim DAC which provides a more consistent long term DAC, at the cost of data delivery delay. This explains why the PSMSL series are shorter for recent missions and do not fully cover 2016.

Overall, the global difference time series obtained with PSMSL are noisier than GLOSS/CLIVAR ones, which directly impacts uncertainty levels. Recent missions seems to be more affected than older ones (for ERS-2 the uncertainty is even lower with PSMSL). This may be due to the fact that GLOSS/CLIVAR network was more tenuous during the early altimetry missions whereas the historical PSMSL database was already very dense. On top of that, the drop of the number of available PSMSL tide gauges on recent dates due to a the longer time delay results larger uncertainties for current missions (SARAL/Altika and Jason-2).

The derived GMSL drifts obtained with PSMSL are relatively close to GLOSS/CLIVAR ones. Except for Jason-1, the difference is lower than the uncertainty obtained with GLOSS/CLIVAR

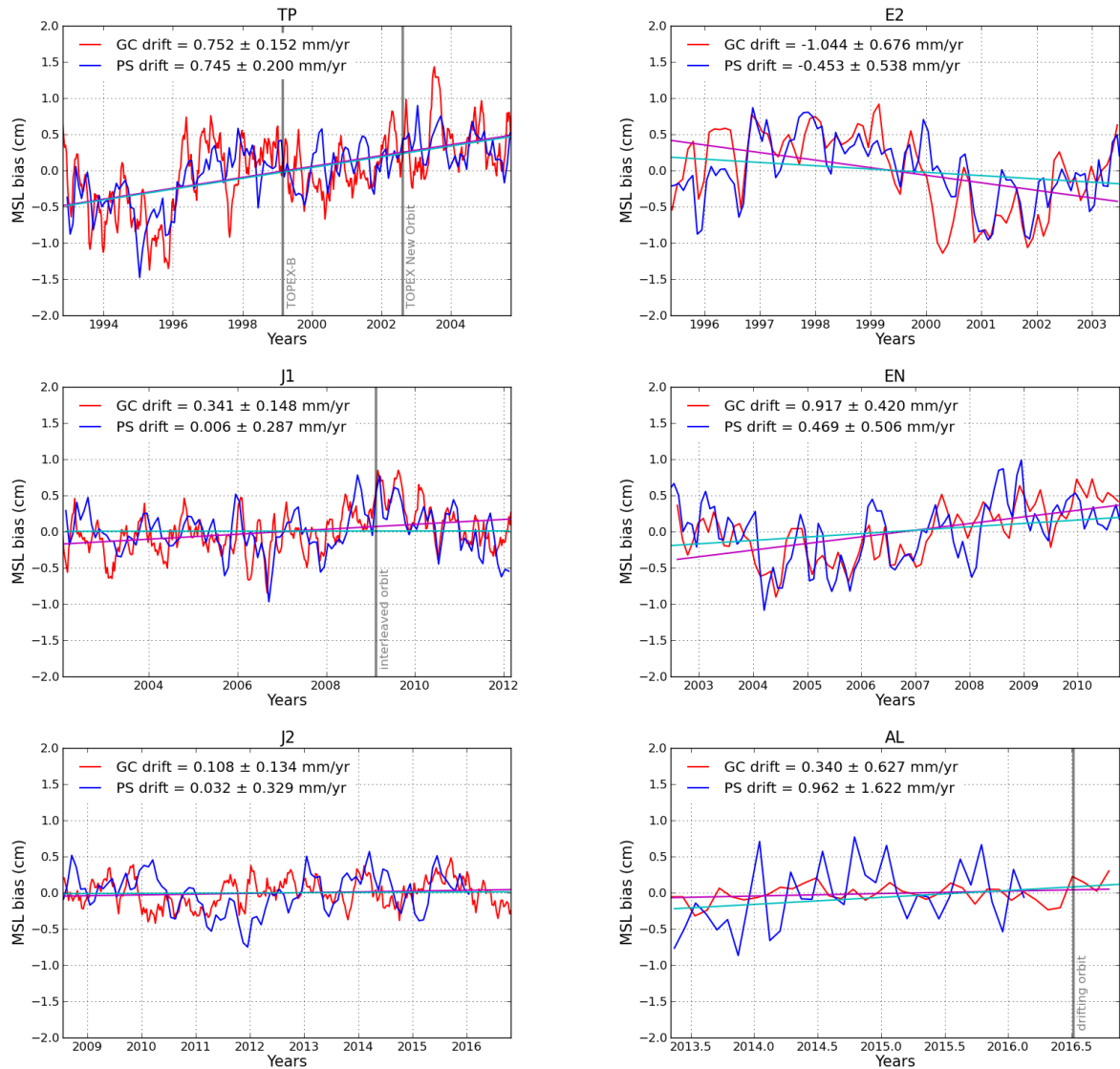


Figure 27: Comparison of PSMSL and GLOSS/CLIVAR drifts derived from altimetry - tide gauges. Each subplot sets for an altimetry mission. On the left, the reference missions TOPEX/Poseidon, Jason-1, Jason-2 from top to bottom. On the right, the long cycle mission ERS-2, Envisat, SARAL/Altika from top to bottom.

network.

These new results based on PSMSL stations are consistent with findings on GLOSS/CLIVAR. They are made possible thanks to improvements in the data processing that allows us to estimate SSH properly on monthly PSMSL data.

5.4. Distance threshold

The correlation grid is computed in a 200 km radius distance from the tide gauge position. this limit should prevent the time serie comparison from being done on a long range colocation due to a fortuitous correlation. Nevertheless, this limit is also responsible for the editing of several tide gauge series due to a vicinity contaminated by coast and/or land pixels. The purpose of this investigation is to assess the influence of this distance limit D_{max} on the results of the altimetry-tide gauges comparison.

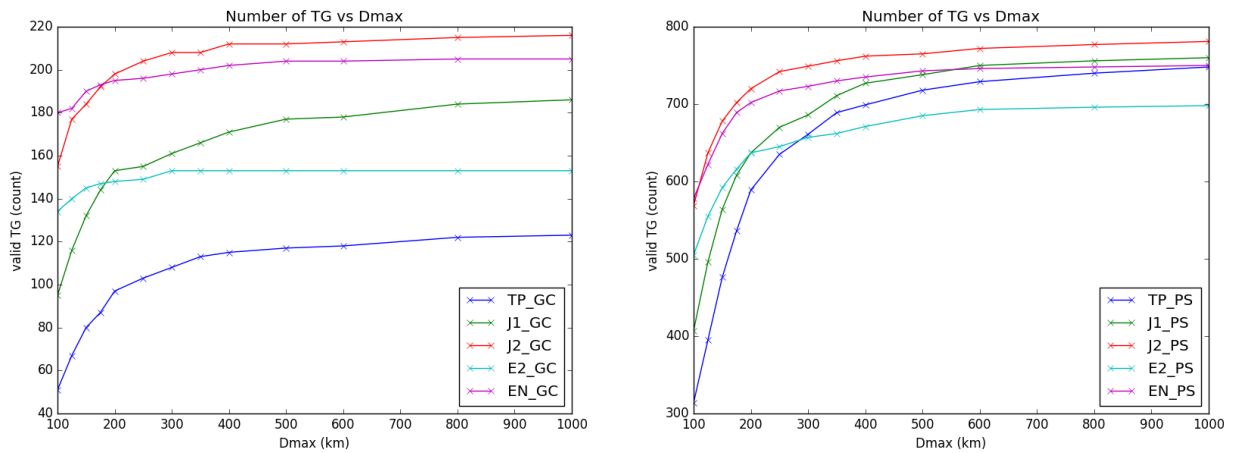


Figure 28: Number of valid tide gauges versus the distance limit of colocation for GLOSS/CLIVAR (left) and PSMSL (right).

Figure 28 displays the variation of the number of valid tide gauges with the distance limit. Obviously, when this limit increases, the number of stations fulfilling the criteria rises too. All curves converge to an asymptotic value, but convergence seems faster for long cycle mission (as soon as $D_{max} > 250$ km) than for short cycle mission ($D_{max} > 600$ km). This is a direct consequence of the different spatial samplings of the ground tracks with 254 versus 1002 tracks covering the full 360° . This suggests that maybe the optimal D_{max} value depends on the mission and that the number of considered tide gauges may be significantly increased for reference missions.

Figure 29 shows how the mean correlation depends on D_{max} . Overall, when D_{max} increases, the average correlation rises but slightly. For both GLOSS/CLIVAR and PSMSL, the variations when passing D_{max} from 100 km to 1000 km do not exceed 0.2. All missions show the same behavior with small variations above $D_{max} = 500$ km.

The way the GMSL drifts and their uncertainties are affected by D_{max} is represented on figure 30. SARAL/Altika's drift is unstable, when compared to GLOSS/CLIVAR or to PSMSL data. We interpret this as a consequence of the short length of the available time serie. For all other missions, the drift variations are lower than 0.3 mm/year when D_{max} goes from 100 km to 1000 km. This is in the uncertainty range. Most of the variations of the drift are observed below 400 km.

Concerning the drift uncertainty, it slightly decreases with D_{max} stabilizes after approximately 200 to 300 km. The trend of this variation truly depends on the mission, it is very weak for the reference missions and more significant for ERS 2 and Envisat (up to 0.1 mm/year from $D_{max} = 100$ km to

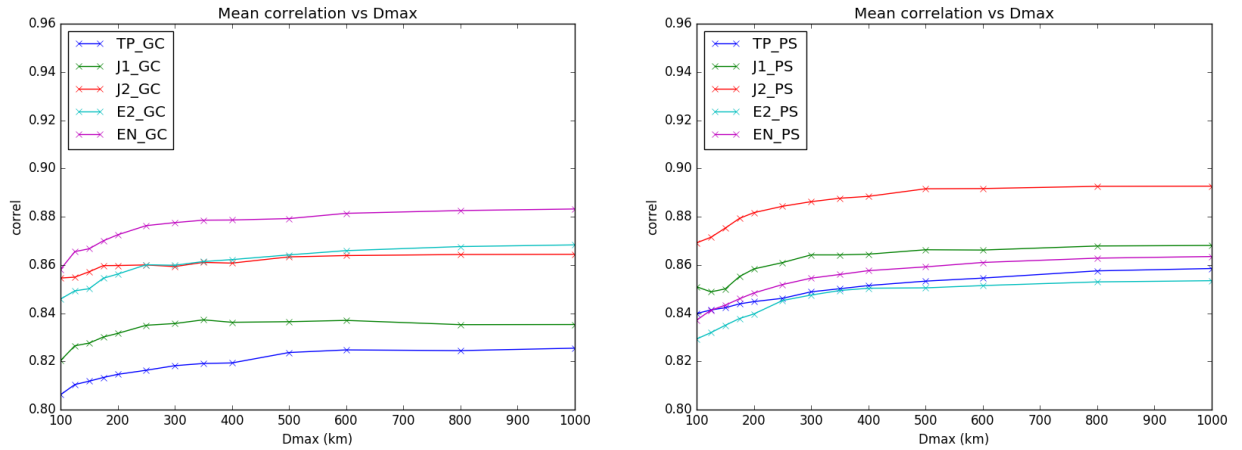


Figure 29: Mean correlation of valid tide gauges versus the distance limit of collocation for GLOSS/CLIVAR (left) and PSMSL (right).

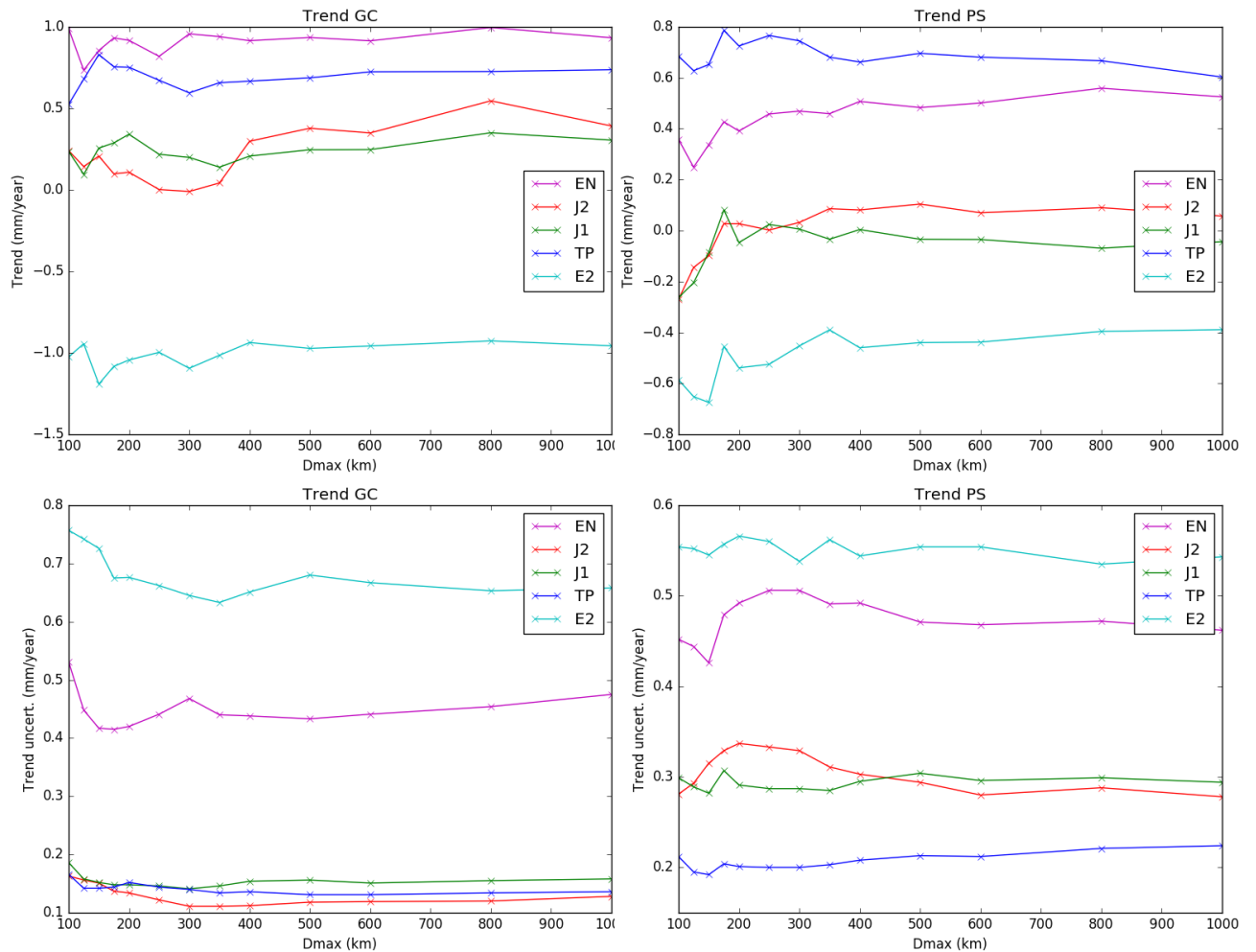


Figure 30: Variation of the GMSL drift between altimetry and tide gauges for GLOSS/CLIVAR (left) and PSMSL (right). On top, the trend obtained by linear regression and on bottom, the trend formal uncertainty.

$D_{max} = 200$ km). On the other hand, when using the PSMSL network there is no clear dependance between the uncertainty and D_{max} .

Overall, this investigation shows that the distance limit of colocation may be increased from the current $D_{max} = 200$ km. Especially for the reference mission, it would increase the number of tide gauges fulfilling the criteria. Furthermore, the average correlation and the drift seems to be more stable with $D_{max} > 400$ km. The disadvantage of this would be to open the gate to fortuitous correlations and the use of longer range of colocation. Further work might investigate on a better selection of the best pixel in the grid, for example using a mixed criteria between correlation and distance to the tide gauge.

5.5. SAR interferometry for VLM characterisation

A large source of uncertainty in global comparisons between satellite altimetry and tide gauges for the detection of long term drifts is the vertical land motion of tide gauges benchmarks. At the moment in our methodology only GIA related VLM are corrected using a model. Last year, we compared global drifts results using GPS vertical velocity rates and using only a GIA model. While GPS data should provide a better knowledge of VLM, and therefore increase the agreement between altimetry and tide gauges, we were unable to demonstrate a positive impact of the use of GPS data ([22]). In a 2013 study, [31, Raucoules et al., 2013] used interferometry between SAR images to estimate ground motion in Manila. Manila has a tide gauge station, and a GPS station is located 1.7 km away. Figure 31, taken from their paper, displays the map of ground motion over the 1993-1998 period. It clearly shows that the GPS and the station, even closely located, experience very different ground motions. Global comparisons between altimetry and tide gauges would benefit from a more complete atlas of such ground motions.

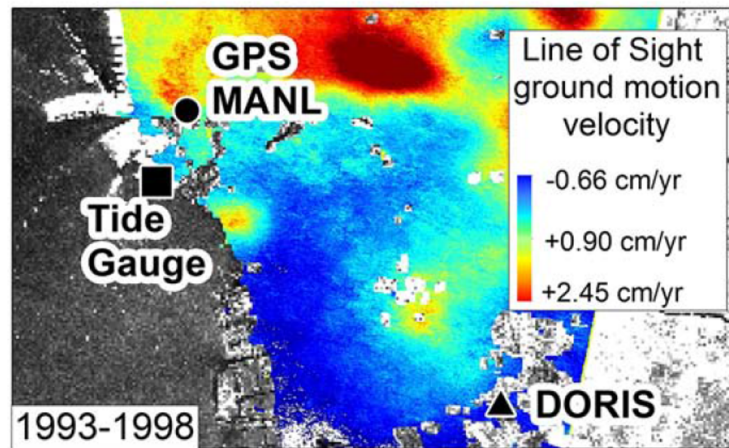


Figure 31: Ground motion inferred from DInSAR in Manila over the 1993-1998 period from [31].

5.6. Drift of a Poseidon based TOPEX record

[33, Zawadzki et al., 2016] proposed a way to correct the TOPEX/Poseidon records using Poseidon data. By doing so, they generated a GMSL record for TOPEX/Poseidon, exhibiting a slightly lower trend. In an attempt to determine which of the reference or the corrected records was right, we performed a comparison to tide gauges measurements. The two records show very similar patterns (they only differ by a long-term drift correction) but the Poseidon calibrated record shows a lower drift with respect to tide gauges. While the reference TOPEX/Poseidon record drifts by 1 mm/yr (which is above the method uncertainty), the Poseidon calibrated record shows a lower drift at -0.36 mm/yr, and is therefore more consistent with tide gauges data. This suggests that using Poseidon to correct TOPEX might actually bring some improvements regarding GMSL stability.

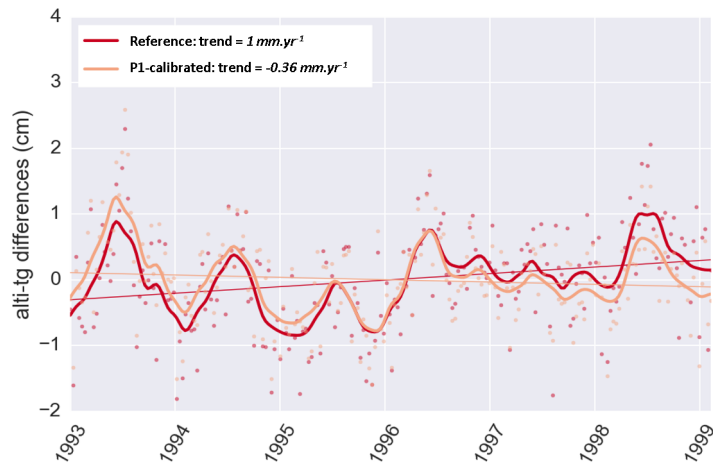


Figure 32: Comparing global bias times series for the current TOPEX/Poseidon record, and for a Poseidon calibrated TOPEX record.

6. Conclusions

This report presents the status of the global comparisons between altimetry and tide gauges, as well as the work and investigations performed in 2016. These activities are supported by CNES through the SALP project. The goal of these comparisons is to detect errors on altimeter records. An important part of this process, although mostly hidden, is to acquire tide gauges data from different data providers. These data are then used as a reference for altimetry comparisons that are updated routinely with new in-situ and altimeter data. Moreover, dedicated studies are undertaken to characterise the performance of the method, or investigate a specific processing aspect.

In 2016, there was a major change in the way we manage tide gauges database and fill them with data:

- three databases are operationnally filled: a monthly one, an hourly one and a high-rate one,
- the hourly database contains all tide gauges series re-sampled to an hourly frequency sampling,
- the hourly re-sampling allows to execute the full processing on any tide gauge serie,
- an altimetry consistent SLA is available for all station whatever is its sampling.

We routinely ingest five networks into CLS tide gauges databases:

- the GLOSS/CLIVAR fast delivery dataset,
- the PSMSL dataset,
- the REFMAR french dataset,
- the CNES Senetosa sites,
- the Copernicus european dataset.

The main objective of the altimetry in-situ comparisons is to detect any drifts or jumps in satellite altimetry time series, and global comparisons results are routinely updated. The main findings from these comparisons are:

- For Jason-2, which was until recently the reference mission for GMSL monitoring, the comparison to tide gauges shows no drift, and demonstrates the excellent stability of the mission.
- Jason-1 doesn't show any statistically significant drift either, yet a jump is still observed on the time series of SSH differences, corresponding to the change to the interleaved orbit.
- TOPEX/Poseidon shows a positive drift, especially in the early part of the record (TOPEX-A). The negative anomaly observed in 1995-1996 could be explained by the application of CAL-1.
- A significant positive trend is still observed on the ENVISAT mission (0.9 mm/year). This positive trend is consistent with global MSL analysis and comparisons to Argo floats.
- SARAL/Altika is included to these comparisons, and shows a particularly low RMS of the differences.

As a follow-on to the analysis performed in 2013, 2014 and 2015, the 2016 investigations have mainly been devoted to the estimation of the sensitivity of the method. The analysis presented in this report focused on:

- The stability of the method used to average the stations and how a different bin shape than the 6° longitude bands may affects the comparison. The results suggested that smaller bins might be more stable.
- A new method aiming to reduce the SNR of altimetry time series, called "multiple pixels". Despite little changes on the global drift uncertainty, it improves clearly the correlation of each individual station time serie with satellite altimetry.
- Global bias time series are estimated using the PSMSL tide gauges, while these comparisons remain noisier than GLOSS/CLIVAR ones, the main patterns are consistent.
- Extending the search radius of colocations between altimetry and tide gauges suggests that an increase from 200 km to 300-400 km would allow to consider more stations especially for the reference missions.

7. References

References

- [1] Ablain, M., S. Philipps, M. Urvoy, N. Tran, and N. Picot, 2012: Detection of long-term instabilities on altimeter backscatter coefficient thanks to wind speed data comparisons from altimeters and models. *Marine Geodesy* 2012, DOI: 10.1080/01490419.2012.718675.
- [2] Ablain, M., A. Cazenave, G. Valladeau, and S. Guinehut, 2009: A new assessment of global mean sea level from altimeters highlights a reduction of global trend from 2005 to 2008. *Ocean Sci. Disc.*, 6, 31-56.
- [3] AVISO, 2013: Envisat RA2/MWR ocean data validation and cross-calibration activities. 2013 annual validation report. SALP-RP-MA-EA-XXXXX-CLS ed. 1.0, 129 pp.
- [4] AVISO, 2013: Jason-2 validation and cross calibration activities. 2013 annual validation report. SALP-RP-MA-EA-22270-CLS ed. 1.0.
- [5] Bessero, G., 1985: *Marées*, Service Hydrographique et Océanographique de la Marine, Brest.
- [6] ESA Sea Level CCI Validation Report, WP2700 Coastal areas, 2011 http://www.esa-sealevel-cci.org/webfm_send/186.
- [7] Legeais, J.F., and P. Prandi, 2013: Validation of altimeter data by comparison with in-situ Argo T/S profiles. SALP-RP-MA-EA-22281-CLS ed. 1.0.
- [8] Bouffard, J., A. Pascual, S. Ruiz, Y. Faugère, and J. Tintoré, 2010: Coastal and mesoscale dynamics characterization using altimetry and gliders: A case study in the Balearic Sea. *J. Geophys. Res.*, 115, C10029, doi:10.1029/2009JC006087.
- [9] Carrère, L. and F. Lyard, 2003: Modeling the barotropic response of the global ocean to atmospheric wind and pressure forcing - comparisons with observations. *Geophys. Res. Lett.*, Vol. 30, 1275, 4 pp. doi:10.1029/2002GL016473.
- [10] Cartwright, D.E., and A.C. Eden, 1973: Corrected Tables of Tidal Harmonic, *Geophys. J. R. Astr. Soc.*, 17 (5), 619-622.
- [11] Doran, Kara J., 2010: Addressing the problem of land motion at tide gauges. Graduate Theses and Dissertations. <http://scholarcommons.usf.edu/etd/1616>
- [12] Dorandeu, J., and P.-Y. Le Traon, 1999: Effects of global mean atmospheric pressure variations on mean sea level changes from Topex/Poseidon, *J. Atmos. Oceanic Technol.*, 16,

1279-1283.

- [13] Labroue, S., 2007 : RA2 ocean and MWR measurement long term monitoring, 2007 report for WP3, Task 2 - SSB estimation for RA2 altimeter. Contract 17293/03/I-OL. CLS-DOS-NT-07-198, 53pp. CLS Ramonville St. Agne
- [14] Prandi, P., G. Valladeau, J.F. Legeais, M. Ablain, and N. Picot, 2013: Analyses of altimetry errors using in-situ measurements: tide gauges and Argo profiles. OSTST, Boulder.
- [15] Peltier, W. R., 2004: Global Glacial Isostasy and the surface of the ice-age earth: the ICE-5G (VM2) Model and Grace. *Annu. Rev. Earth Planet. Sci.*, 32 (2004), pp. 111-149.
- [16] Peltier, W. R., D.F. Argus and R. Drummond, 2015: Space geodesy constrains ice-age terminal deglaciation: The global ICE-6G (VM5a) model. *J. Geophys. Res. Solid Earth*, 120, 450-487, doi:10.1002/2014JB011176.
- [17] Ruiz Etcheverry, L. A., M. Saraceno, A. R. Piola, G. Valladeau, and O. O. Möller: Annual cycle in coastal sea level from gridded satellite altimetry and tide gauges. *Continental Shelf Research*, in press.
- [18] Specific Works and Studies done during year 2014 within DUACS/GIM Expertise and Quality Activities, 2015, ref: CLS-DOS-NT-14-264/SALP-RP-MA-EA-22401-CLS
- [19] Tamisiea, M.E., and J.X. Mitrovica, 2011: The moving boundaries of sea level change: Understanding the origins of geographic variability. *Oceanography* 24(2):24–39.
- [20] Validation of altimeter data by comparison with tide gauge measurements: yearly report 2013, ref: CLS-DOS-NT-13-285/SALP-RP-MA-EA-22294-CLS
- [21] Validation of altimeter data by comparison with tide gauge measurements: yearly report 2014, ref: CLS-DOS-NT-15-020/SALP-RP-MA-EA-22419-CLS
- [22] Validation of altimeter data by comparison with tide gauge measurements: yearly report 2015, ref: CLS-DOS-NT-15-062/SALP-RP-MA-EA-22958-CLS
- [23] Valladeau, G., J.F. Legeais, M. Ablain, P. Prandi, N. Picot, P. Femenias, and J. Benveniste, 2013: Analyses of altimetry errors using in-situ measurements: tide gauges and Argo profiles. ESA Living Planet Symposium, Edimbourg.
- [24] Valladeau, G., J.F. Legeais, M. Ablain, S. Guinehut, and N. Picot, 2012: Comparing altimetry with tide gauges and Argo profiling floats for data quality assessment and Mean Sea Level studies. *Marine Geodesy* 2012, DOI: 10.1080/01490419.2012.718226.

- [25] Valladeau, G., L. Soudarin, M. Gravelle, G. Wöppelmann, and N. Picot, 2013: Quality assessment of altimeter and tide gauge data for Mean Sea Level and climate studies.
- [26] Zeilis, A., C. Kleiber, W. Krämer, and K. Hornik, 2003: Testing and dating of structural changes in practice. *Computational Statistics & Data Analysis* 44 (2003) 109 – 123.
- [27] Zeilis, A., A. Shah and I. Patanaik, 2010: Testing, monitoring and dating structural changes in exchange rate regimes. *Computational Statistics & Data Analysis* 54 (2010) 1696 – 1706.
- [28] Watson, C. S., N. J. White, J. A. Church, M. A. King, R. J. Burgette, B. Legresy, 2015: Unabated global mean sea-level rise over the satellite altimeter era. *Nature Climate Change*, 5, 565–568.
- [29] Jevrejeva, S., J. C. Moore, A. Grinsted, P. L. Woodworth, 2008: Recent global sea level acceleration started over 200 years ago? *Geophysical Research Letters*, vol. 35, L08715.
- [30] Callahan, P., J. McMichael, B. A. Williams, D. Vandemark, H. Feng, 2015: Retracked TOPEX Climate Data Record Summary, presentation at OSTST 2015.
- [31] Raucoules, D., G. Le Cozannet, G. Wöppelmann, M. De Michele, M. Gravelle, et al., 2013, High nonlinear urban ground motion in Manila(Philippines) from 1993 to 2010 observed by DInSAR: implications for sea-level measurement. *Remote Sensing of Environment*, 139, pp.386-397.
- [32] Beckley, B. D., R.D. Ray, G. T. Mitchum and D. Hancock, 2016, On the “cal mode” correction to TOPEX altimetry and its effect on the global mean sea-level time series, Ocean Surface Topography Science Team Meeting
- [33] Zawadzki, L., M. Ablain, P. Thibaut and P. Prandi, 2016, Estimating a drift in TOPEX-A Global Mean Sea Level using Poseidon-1 measurements, Poster, OST/ST Meeting

8. Appendix

8.1. Standard DUACS 2014

All altimetry SLA used in comparaison with tide gauges are built using the following corrections.

L2P 2014	ERS-1	ERS-2	EN	T/P	J1	J2	GFO	C2	AL	H2	J3
Orbit	Reaper	Reaper	GDR-D	GFSC STD08	GDR-D	GDR-D	GSFC	GDR-D	GDR-D	GDR-D	GDR-E
Major Instrumental correction			PTR FPAC							Correction Doppler	
Sea State Bias	BM3 (Gaspar, Ogor, 1994)	Non parametric Mertz et al., 2005	Tran 2012 compatible enhanced MWR	Non parametric SSB [N. Tran and al. 2010]	Tran 2012 (présenté à l'OSTST)	Tran 2012	Non parametric SSB [N. Tran and S. Labroue]	Non parametric SSB de J1 (des GDR-C) avec sigé débiaisé	Tran 2012	Non parametric SSB [N. Tran] (Vent Labroue)	Tran 2012
Ionosphere	Reaper	Bent (cycle 1-49), GIM from cycle 50	Iono filtre SLOOP / GIM (GDR2.1)	Iono filtre SLOOP	Iono filtre SLOOP	Iono filtre SLOOP	GIM	GIM	GIM	GIM	Iono filtre SLOOP
Wet troposphere	MWR	Minimisation of brightness temperature drift [Scharoo et al. 2004]	MWR replacement product + algo composite	TMR (Scharoo et al. 2004)	MWR replacement product + algo composite	GDR-D (MWR JPL enhancement product)	From GFO radiometer	From ECMWF model	From AL radiometer	From ECMWF model	From J3 radiometer
Dry troposphere	Era Interim based		ECMWF Gaussian grids based	Era Interim based	ECMWF rectangular grids based	ECMWF Gaussian grids based	ECMWF rectangular grids based	ECMWF Gaussian grids based	ECMWF Gaussian grids based	ECMWF Gaussian grids based	ECMWF Gaussian grids based
Combined atmospheric correction	Era Interim based		MOG2D High Resolution forced with ECMWF pressure and wing fields + IB	Era Interim based	MOG2D High Resolution forced with ECMWF pressure and wing fields + IB			MOG2D High Resolution forced with ECMWF pressure and wing fields + IB from rectangular grids	MOG2D High Resolution forced with ECMWF pressure and wing fields + IB	MOG2D High Resolution forced with ECMWF pressure and wing fields + IB	MOG2D High Resolution forced with ECMWF pressure and wing fields + IB
Ocean tide	GOT4V8 (choix pour produit global au moins, à confirmer pour produits régionaux)										
Solid Earth tide	Elastic response to tidal potential [Cartwright and Tayler, 1971],[Cartwright and Edden, 1973]										
Pole tide	[Wahr, 1985]										
MSS	CNES-CLS-2011 + reference period changed										

Figure 33: Altimetry Standards